*Geological Magazine*

**www.cambridge.org/geo**

# Petrogenesis of the peralkaline Flowers River Igneous Suite and its significance to the development of the southern Nain Batholith

Taylor A. Ducharme[1], Christopher R.M. McFarlane[1], Deanne van Rooyen[2] and David Corrigan[3]

[1]Department of Earth Sciences, University of New Brunswick, Fredericton, NB, E3B 5A3, Canada; [2]Department of Mathematics, Physics, and Geology, Cape Breton University, Sydney, NS, B1P 6L2, Canada and [3]Geological Survey of Canada, Ottawa, ON, K1A 0E8, Canada

**Original Article**

**Cite this article:** Ducharme TA, McFarlane CRM, van Rooyen D, and Corrigan D (2021) Petrogenesis of the peralkaline Flowers River Igneous Suite and its significance to the development of the southern Nain Batholith. *Geological Magazine* **158**: 1911–1936. https://doi.org/10.1017/S0016756821000388

Received: 29 November 2020
Revised: 2 April 2021
Accepted: 7 April 2021
First published online: 20 May 2021

**Keywords:**
Peralkaline granite; Nain Plutonic Suite; AMCG magmatism; U–Pb zircon geochronology; Proterozoic magmatism

**Author for correspondence:** Taylor A. Ducharme, Email: taylor.ducharme@unb.ca

## Abstract

The Flowers River Igneous Suite of north-central Labrador comprises several discrete peralkaline granite ring intrusions and their coeval volcanic succession. The Flowers River Granite was emplaced into Mesoproterozoic-age anorthosite–mangerite–charnockite–granite (AMCG) -affinity rocks at the southernmost extent of the Nain Plutonic Suite coastal lineament batholith. New U–Pb zircon geochronology is presented to clarify the timing and relationships among the igneous associations exposed in the region. Fayalite-bearing AMCG granitoids in the region record ages of 1290 ± 3 Ma, whereas the Flowers River Granite yields an age of 1281 ± 3 Ma. Volcanism occurred in three discrete events, two of which coincided with emplacement of the AMCG and Flowers River suites, respectively. Shared geochemical affinities suggest that each generation of volcanic rocks was derived from its coeval intrusive suite. The third volcanic event occurred at 1271 ± 3 Ma, and its products bear a broad geochemical resemblance to the second phase of volcanism. The surrounding AMCG-affinity ferrodiorites and fayalite-bearing granitoids display moderately enriched major- and trace-element signatures relative to equivalent lithologies found elsewhere in the Nain Plutonic Suite. Trace-element compositions also support a relationship between the Flowers River Granite and its AMCG-affinity host rocks, most likely via delayed partial melting of residual parental material in the lower crust. Enrichment manifested only in the southernmost part of the Nain Plutonic Suite as a result of its relative proximity to multiple Palaeoproterozoic tectonic boundaries. Repeated exposure to subduction-derived metasomatic fluids created a persistent region of enrichment in the underlying lithospheric mantle that was tapped during later melt generation, producing multiple successive moderately to strongly enriched magmatic episodes.

## 1. Introduction

Peralkaline igneous rocks exhibit a wide degree of morphological, mineralogical and compositional variation; for this reason, there have been numerous models proposed to explain their modes of genesis (e.g. Whalen *et al.* 1987; Martin, 2006; Markl *et al.* 2010; Frost & Frost, 2011; Vasyukova & Williams-Jones, 2020). Despite their diversity, peralkaline rocks share certain common attributes including enrichment in incompatible lithophile and high-field-strength elements and a broad spatial association with intracratonic rift settings (Sørensen, 1992; Dostal, 2016). It is widely accepted that peralkaline magmas represent highly fractionated liquids originating either from low degrees of partial melting in the mantle or from a previously enriched crustal or mantle source (Martin, 2006; Dostal, 2016; Marks & Markl, 2017). In the latter scenario, enrichment is commonly purported to arise from focused metasomatism beneath a region of the lithosphere undergoing extension, or from an upwelling mantle plume (Martin, 2006; Shellnutt & Zhou, 2007). However, permissible timescales for the introduction of these volatiles remain uncertain and, for voluminous peralkaline intrusions otherwise lacking evidence of plume involvement, the extent of the enrichment imposed on the source region must be considerable.

In Labrador, there exists an atypical but systematic spatial relationship between peralkaline intrusions and anorthosite–mangerite–charnockite–granite (AMCG) -affinity rocks of the Nain Plutonic Suite (Fig. 1; Kerr, 2011). The Nain Plutonic Suite is one of the largest exposures of AMCG-affinity rocks worldwide (Emslie, 1978; Emslie *et al.* 1994; Myers *et al.* 2008; Ashwal & Bybee, 2017). These igneous complexes are at the core of many enduring petrologic debates, concerned primarily with how to generate their considerable volumes of anorthosite (Bowen, 1917; Emslie, 1978; Ashwal, 1993; Longhi *et al.* 1999), and how to generate the ubiquitous assortment of coeval accessory lithologies including mangerite, charnockite, rapakivi granite and ferrodiorite (Emslie *et al.* 1994; Scoates *et al.* 1996; Frost & Frost, 1997, 2008b; Vander



CAMBRIDGE UNIVERSITY PRESS

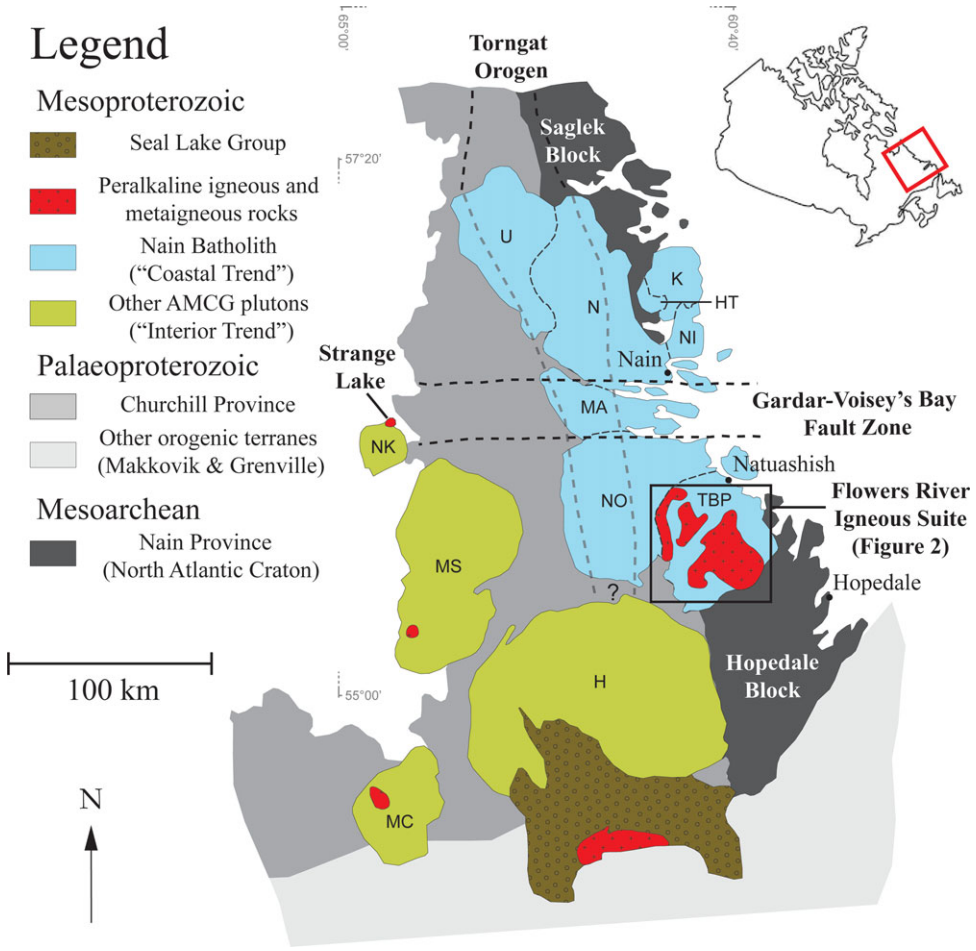


**Fig. 1.** (Colour online) Regional map of Labrador showing the Nain Plutonic Suite's Coastal and Interior Trend AMCG associations as well as major structural corridors in the region. Peralkaline igneous centres are shown in red. H – Harp Lake intrusion; HT – Hettasch intrusion; K – Kiglapait intrusion; MA – Makhavinekh pluton; MC – Michikamau intrusion; MS – Mistastin Batholith; N – Nain anorthosite; NI – Newark Island intrusion; NK – Napeu Kainiut quartz monzonite; NO – Notakwanon Batholith; TBP – Three Bays Pluton; U – Umiakovik Batholith. Modified from Emslie *et al.* (1994) and Kerr (2011). Pluton abbreviations after Emslie *et al.* (1994). Inset area is shown in detail in Figure 2.

Auwera *et al.* 1998; Vigneresse, 2005; Duchesne *et al.* 2017). It has become largely accepted that the 'massif-type' anorthosite in AMCG complexes was formed by segregation of buoyant plagioclase cumulates from a basaltic melt ponded in the lower crust (Emslie, 1978; Morse, 1982; Ashwal, 1993) in tectonic settings associated with either syn- to post-collisional removal of mantle lithosphere (e.g. Corrigan & Hanmer, 1997; McLelland *et al.* 2010), or post-orogenic collapse (e.g. Vander Auwera *et al.* 2011). However, the source of this parental magma remains controversial. Some researchers favour a mantle origin for these melts (Mitchell *et al.* 1996; Frost *et al.* 2010; Bybee *et al.* 2014; Ashwal & Bybee, 2017), whereas others have argued for a lower crustal source (Duchesne *et al.* 1999; Longhi, 2005; Bédard, 2009; Vander Auwera *et al.* 2011; Duchesne *et al.* 2017). A similar debate has developed in parallel concerning the source of, and interrelation between, the accompanying granitoids and ferrodiorites (Emslie *et al.* 1994; Scoates *et al.* 1996; Frost & Frost, 1997, 2013; McLelland *et al.* 2004; Ashwal & Bybee, 2017; Duchesne *et al.* 2017).

The Nain Plutonic Suite diverges from the established petrogenetic framework of AMCG complexes in several key regards. The Nain Plutonic Suite was not emplaced following any direct regional orogenesis (e.g. Corrigan *et al.* 2000; Gower & Krogh, 2002), and therefore cannot have been produced in a post-collisional setting. The ages recorded by the Nain Plutonic Suite also suggest that it was an unusually long-lived magmatic system. Magmatism occurred in two distinct episodes, yielding an older suite (1460–1420 Ma) to the west and a younger suite (1362–1290 Ma) to the east (Miller *et al.* 1997; Myers *et al.* 2008; Fig. 1), whereas emplacement windows for AMCG suites elsewhere have been estimated to span fewer than *c.* 10 Ma (e.g. Schärer *et al.* 1996; Scoates & Chamberlain, 2002; McLelland *et al.* 2004). Some authors propose a connection between Nain plutonism and prolonged convergence along the southern Laurentian margin to accommodate these differences (e.g. Myers *et al.* 2008; Hynes & Rivers, 2010; McLelland *et al.* 2010), but the precise tectonic mechanism underlying magmatism in the region has not yet been fully constrained. Some degree of structural control on magmatic emplacement is evident in the confluence between the eastern Nain Plutonic Suite intrusions and the Torngat Orogen, which defines the boundary between the Archean Nain and Palaeoproterozoic Churchill Provinces (Fig. 1; Myers *et al.* 2008).

The relationship between the peralkaline rocks and their AMCG-affinity host plutons remains uncertain (e.g. Kerr, 2014; Ryan *et al.* 2017), though many of the intrusions have been the subjects of only preliminary reconnaissance (Kerr, 2011). These intrusions therefore constitute a presently underutilized source of

https://doi.org/10.1017/S0016756821000388 Published online by Cambridge University Press

insight into the geodynamic conditions coincident with their emplacement, and potentially that of their AMCG-affinity host plutons. The *c.* 1240 Ma Strange Lake intrusion (Fig. 1) is the most renowned of Labrador's peralkaline complexes (e.g. Miller *et al.* 1997; Salvi & Williams-Jones, 1996; Vasyukova & Williams-Jones, 2014). Isotopic data indicate the Strange Lake intrusion was not derived directly from its host AMCG-affinity pluton (Siegel *et al.* 2017), but the precise relationship between these two intrusions remains incompletely understood, and the Strange Lake intrusion may post-date the earlier intrusion by as much as 200 Ma (Miller *et al.* 1997). By contrast, chronometric data suggest peralkaline granite belonging to the Flowers River Igneous Suite (FRIS; Fig. 1) was emplaced at most 20 Ma after its AMCG-affinity host intrusions (Hill, 1991; Myers *et al.* 2008). This relatively short delay between the two events suggests that the FRIS is more likely to have been influenced by the geodynamic conditions that persisted following the emplacement of its host intrusion. The large size and strong silica-oversaturation of the FRIS preclude low-degree partial melting as a mechanism for its formation, and there is no systematic age progression within the Nain Plutonic Suite to support the involvement of a mantle plume.

The current petrochronological framework for the Flowers River peralkaline granite suggests that it is the youngest magmatic phase within the eastern (younger) composite batholith of the Nain Plutonic Suite that was emplaced along the tectonic boundary dividing the Nain and Churchill Provinces (Hill, 1991; Miller, 1993; Myers *et al.* 2008). The lack of available geochronology for the host rocks to the Flowers River intrusions has impeded a complete understanding of the local magmatic history. This study presents new U–Pb zircon geochronology for the Flowers River Granite, its coeval volcanic succession and the surrounding AMCG-affinity granitoids. These results are combined with whole-rock geochemical data to construct a geodynamic model describing each successive episode of magmatism in the study area. The AMCG-affinity granitoids and ferrodiorites in the Flowers River area show moderately enriched major- and trace-element signatures relative to other AMCG-affinity rocks found elsewhere in the Nain Plutonic Suite. Episodic, comparatively enriched magmatism at a single focal centre over at least 10 Ma precludes a sub-lithospheric source, as such a source would be transient over these timescales. We therefore suggest that either the FRIS was sourced by delayed re-melting of the recently emplaced AMCG-affinity rocks, or that both suites sampled a static enriched reservoir located in the subjacent lithosphere (e.g. Goodenough *et al.* 2002; Upton, 2013; Siegel *et al.* 2017). Massif anorthosite and associated lithologies were generated in large volumes across a wide area during emplacement of the Nain Plutonic Suite and spanned many distinct crustal regimes. Other peralkaline complexes associated with AMCG-affinity magmatism in Labrador may similarly represent the ultimate products of melts sourced from pockets of enriched lithosphere created during earlier Palaeoproterozoic tectonism.

## 2. Geological setting

The Flowers River Igneous Suite intrudes the southernmost region of the eastern division of the Nain Plutonic Suite, a series of AMCG-affinity intrusions distributed throughout Labrador and eastern Québec (Hill, 1982, 1991). The eastern subset of the Nain Plutonic Suite is a large composite batholith that occupies much of the modern coastline of Labrador, referred to here as the Nain Batholith. The Nain Batholith consists of numerous overlapping plutons emplaced during 1362–1290 Ma (Fig. 1; Myers *et al.* 2008). The surface expressions of these plutons expose variable proportions of the various AMCG association lithologies (Emslie, 1978), which has been speculated to reflect preservation at contrasting structural levels spanning a largely uniform initial pluton cross-section (Ryan, 1991; Kerr & Smith, 2000).

The Nain Batholith was emplaced along the Palaeoproterozoic Torngat Orogen, and is transected by the Gardar–Voisey's Bay Fault Zone. These major structural corridors played a major role in facilitating magmatic ascent (Myers *et al.* 2008; McLelland *et al.* 2010). The Nain Batholith is bound to its west by Archean–Palaeoproterozoic gneisses of the Churchill Province, variably reworked by the Torngat Orogeny (Ryan, 2000). Along the coast, the Nain Batholith separates two major Archean crustal blocks: the Hopedale Block to the south and the Saglek Block to the north (Fig. 1). Collision between these two blocks at *c.* 2550 Ma during amalgamation of the North Atlantic Craton formed a wide suture zone, the thermal imprint of which is preserved in remnant exposures of Archean gneiss dispersed within the archipelagic eastern margins of the Nain Batholith (Connelly & Ryan, 1996). The suture itself may have acted as an additional focal conduit for Mesoproterozoic plutonism, though the structure has been largely obscured by the intrusions.

The AMCG-affinity rocks that host the FRIS have been divided previously into three anorthositic plutons: the Sango Bay Pluton, Merrifield Bay Pluton and Flowers Bay Pluton (Hill, 1988; Fig. 2). Hypersolvus, fayalite-bearing granite and monzonite occur in approximately equal proportion to the anorthositic lithologies. These granitoids are interpreted to be equivalent to the hypersthene-bearing charnockite and mangerite prevalent throughout the Nain Plutonic Suite, although emplaced at comparatively lower pressures or crystallized from magmas with high Fe/Mg (Le Maitre *et al.* 2005; Frost & Frost, 2008*b*). For simplicity, the three anorthositic bodies and their coeval fayalite-bearing granitoids are collectively referred to here as the 'Three Bays Pluton' (TBP). The TBP lies to the immediate SE of the Notakwanon Batholith, a predominantly granitic AMCG-affinity intrusion with approximately equal proportions of classic hypersthene-bearing (charnockite *sensu stricto*) and fayalite-bearing granitoids (Hill, 1982; Emslie & Stirling, 1993). Previous work on the Notakwanon Batholith has shown that its granitoid rocks display more pronounced Eu and Sr depletion than more northerly Nain Batholith intrusions (Emslie & Stirling, 1993). There are currently no geochronological data available for the Notakwanon Batholith, but it is inferred to be slightly older than the FRIS (Myers *et al.* 2008).

The Flowers River Igneous Suite comprises the Flowers River peralkaline granite and the coeval Nuiklavik volcanic succession. The Flowers River Granite is the largest peralkaline intrusive body in Labrador, and forms an extensive series of intrusions ($> 2000\ km^2$ mapped surface area) with arcuate to curvilinear geometry dispersed throughout the Three Bays Pluton and emplaced concentrically around the Nuiklavik caldera (Hill, 1982; Fig. 2). Medium-grained equigranular peralkaline granite is the primary constituent of the intrusions, with sparse porphyritic and pegmatitic expressions near the roof of the pluton, and minor confinement fabrics developed locally along pluton margins (Hill, 1982, 1991). The coeval Nuiklavik Volcanics have attracted interest due to localized radiometric anomalies and coincident Zr–Y–Nb–REE (rare earth element) mineralization (Hill, 1982; Miller, 1992, 1993). The Nuiklavik caldera is a roughly circular feature *c.* 10 km in diameter, located at the centre of the largest peralkaline granite intrusion, toward the southeastern extent of the study area (Fig. 1;

https://doi.org/10.1017/S0016756821000388 Published online by Cambridge University Press

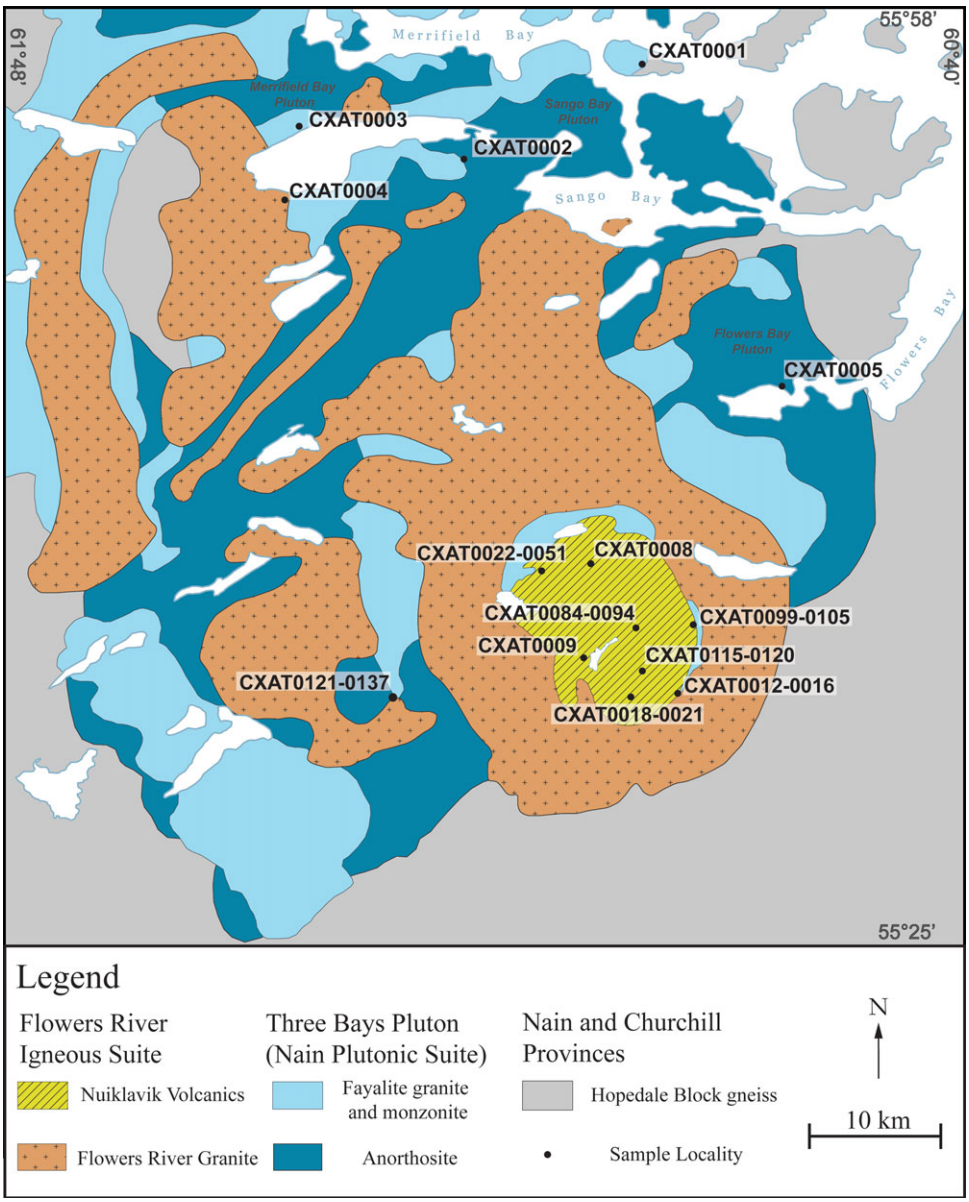


**Fig. 2.** (Colour online) Geological map of the Three Bays Pluton and Flowers River Igneous Suite. Individual plutons are marked as named by Hill (1988). Modified after Hill (1982).

Hill, 1982). The volcanic succession comprises a diverse array of silicic volcanic lithofacies including crystal-rich to aphyric ash flows, ignimbrites and porphyries, as well as possible lavas and subvolcanic domes (Miller, 1992, 1993). The Nuiklavik Volcanics occupy a depression in the central Flowers River Granite intrusion, and windows of peralkaline granite are dispersed throughout the caldera. Volcanic rocks also lie in direct contact with inliers of fayalite granite and monzonite around the caldera edges. Pristine preservation of primary volcanic textures is common, although intense alteration frequently accompanies mineralization and may overprint these textures. Widespread, extreme Na depletion has been documented in the Nuiklavik Volcanics (Miller, 1994), and few samples preserve mineralogical or geochemical evidence for an initially peralkaline composition. Nevertheless, trace-element compositions appear consistent with the volcanic rocks having been derived from the Flowers River magmas (Miller, 1992).

The geochronological framework for the Flowers River area is poorly defined. Emplacement timings for the Three Bays Pluton, along with the nearby Notakwanon Batholith (Fig. 1), have previously been inferred based on ages reported for the FRIS (Emslie & Stirling, 1993; Myers *et al.* 2008). The timing of Flowers River magmatism is better constrained, but the various reported ages span a considerable range. Collerson (1982) first reported a Rb–Sr errorchron age of 1262 ± 7 Ma for peralkaline granites located near Flowers Bay, at the northwestern edge of the study area. Later thermal ionization mass spectrometry (ID-TIMS) U–Pb zircon dating reported two ages, 1291 ± 2 and 1289 ± 1 Ma, for a Nuiklavik porphyry (Miller, 1994), and three zircon fractions yielded an age of 1271 ± 15 Ma for the Flowers River Granite (Hill, 1991). Additional geochronological data would serve to clarify the relationship between the Flowers River Granite and the Nuiklavik Volcanics, as well as to determine a timing of emplacement for the Three Bays Pluton.

https://doi.org/10.1017/S0016756821000388 Published online by Cambridge University Press

As noted above, the spatial association observed between peralkaline intrusions and earlier AMCG-affinity plutons in Labrador (e.g. Miller *et al.* 1997; Kerr, 2011) is not a systematic component of AMCG complexes elsewhere. An exception to this is the Mount Rosa complex in Colorado, a late-stage intrusion within the Pikes Peak Batholith (Barker *et al.* 1975; Smith *et al.* 1999). The geodynamic conditions that fostered AMCG magmatism have also been noted to resemble those corresponding to Mesozoic peralkaline magmatism in Nigeria (Magaji *et al.* 2011; Martin *et al.* 2012), and the Gardar alkaline province in Greenland is inferred to sit atop an extensive AMCG complex (Bridgwater, 1967; Upton *et al.* 2003). All of these examples are similarly far removed in time from their most recent instances of regional orogenesis as the Nain Plutonic Suite. Notably, the Gardar Province is similar in age to the peralkaline intrusions in Labrador, and would have been directly adjacent to these localities around the time of their emplacement (e.g. Blaxland & Parsons, 1975; Waight *et al.* 2002; McCreath *et al.* 2012; H Salmon, unpub. Ph.D. thesis, University of London, 2013; Upton, 2013; Borst *et al.* 2019).

## 3. Sampling and analytical methods

Samples of both Three Bays Pluton and Flowers River intrusive lithologies were obtained from near the outer ring segments or at the margins of the central Flowers River intrusion (Fig. 2). A total of 37 samples were selected for whole-rock geochemical analysis, and between 400 and 1000 g of material was provided for processing. Geochemical analyses were provided by Activation Labs in Ancaster, Ontario using lithium borate fusion inductively coupled plasma optical emission spectrometry (ICP-OES) and mass spectrometry (ICP-MS) for major- and trace-element analyses, respectively. Analytical uncertainties obtained using these techniques are less than 1%. These data were supplemented with geochemical data obtained previously by the Newfoundland Department of Mines and Energy for the Nuiklavik Volcanics (Miller & Kerr, 2007).

Conventional petrographic mineral identification was supported by backscatter electron (BSE) imaging and energy-dispersive spectroscopy (EDS) using a JEOL 6400 scanning electron microscope (SEM) at the University of New Brunswick's Microscopy and Microanalytical Facilities.

Laser ablation (LA-) ICP-MS was conducted at the University of New Brunswick using a Resonetics S-155-LR ArF Excimer laser system along with an Agilent Technologies 7700× quadrupole ICP-MS. Zircon analyses were performed *in situ* (e.g. McFarlane & Luo, 2012) with on-sample fluence of 3 J $cm^{-2}$ and a repetition rate of 3 Hz. Zircon specimens were ablated for 30 second intervals for the collection of U–Pb data, and for 60 second intervals for simultaneous collection of geochronological and trace-element data. Ablation crater diameter varied between 33 and 45 μm depending on the modal size of zircon grains. The primary zircon geochronological standard used was FC-1, with Plesovice and 91500 serving as secondary standards. Instrument tuning was performed prior to each analytical session using synthetic glass standard NIST-610. Standard U–Pb ages were reproducible to within 1% of the true age of the material.

## 4. Lithological descriptions and geochemistry

### 4.a. Three Bays Pluton

Fayalite-bearing granitoids constitute the majority of AMCG-affinity rocks exposed in the vicinity of the Nuiklavik caldera. Fayalite granite and monzonite were found primarily along the caldera margin, but highly altered examples are also exposed in windows along high-elevation ridges. Fayalite granite weathers to a dull orange-brown in outcrop, and easily disintegrates into loose K-feldspar crystals. Fresh surfaces have a paler, pink-orange hue. In thin-section, the granite contains abundant pale green augite and mesoperthite, with subordinate olivine undergoing incipient alteration to iddingsite and/or grunerite (Fig. 3a). Fayalite granite in the immediate vicinity of the caldera has deeper green, weakly to moderately pleochroic augite with greater aegirine component, and minor sodic-calcic amphibole. Monzonitic rocks are pale grey to white in outcrop, and weather to a dull white or buff colour. Fayalite monzonite is distinguished from fayalite granite by its finer perthitic exsolution, smaller pale brown augite crystals, plagioclase content and common fully pseudomorphed olivine. They show greater degrees of alteration, with decussate pale green hornblende and biotite as the dominant ferromagnesian minerals. A greater variety of lithologies were encountered along the margins of the central Flowers River pluton, distal to the caldera. These include anorthosite, leucogabbro, granite, and a microperthite- and biotite-bearing ferrodioritic rock resembling ferromonzogabbro or a melanocratic jotunite (a charnockite group designation for ferrodioritic rocks; e.g. Duchesne & Wilmart, 1997; Vander Auwera *et al.* 1998; Fig. 3b). This ferrodiorite appears to be equivalent to the transitional to alkalic ferrogabbro described by Hill (1988), and contains abundant euhedral apatite as well as an unaltered assemblage of olivine, orthopyroxene, clinopyroxene, biotite, plagioclase, apatite and microperthitic alkali feldspar. By contrast, the anorthosite suite lithologies encountered in this study (ranging from leucogabbro to anorthosite *sensu stricto*) comprise plagioclase and clinopyroxene alongside a secondary mineral assemblage of prehnite, calcite, hornblende, epidote and chlorite.

Geochemical data for Three Bays Pluton lithologies are presented in Table 1. All Three Bays granitoids plot as A-type (Fig. 4). Three Bays Pluton fayalite granite displays markedly ferroan compositions, whereas fayalite monzonite is magnesian (Fig. 5a). Three Bays Pluton granitoids unambiguously plot as type $A_2$ granites of Eby (1992; Fig. 5b) and show relatively homogeneous REE and trace-element profiles (Fig. 6). These rocks show moderate to pronounced negative Eu anomalies ($Eu/Eu^* = 0.21–0.55$), flat heavy REE (HREE) trends ($Dy/Yb = 0.94–1.13$), slight relative depletion in Sr, P, Ti and Ba, and variable Nb–Ta troughs. These closely resemble results of prior geochemical analyses of the Notakwanon Batholith (Emslie *et al.* 1994; Fig. 1). Gabbroid members of the TBP deviate from this trend. Ferrodiorite retains a slight negative Eu anomaly ($Eu/Eu^* = 0.7$) and depletion in Sr, but shows moderate enrichment in Ba and Ti with pronounced enrichment in P. The anorthositic rocks display a positive (or no) Eu anomaly ($Eu/Eu^* = 1.04–1.69$), are Ba-enriched and are depleted relative to all other lithologies. Ferrodiorite and anorthositic lithologies are omitted from Figures 4 and 5 because the diagrams used are determined using the geochemical properties of granitoid rocks only.

### 4.b. Flowers River Granite

The Flowers River Granite exhibits textural and mineralogical homogeneity and typically occurs as medium-grained pink to pink-white granite. It locally occurs as thin (< 1 m) pegmatitic veins intruding TBP anorthosite, especially near the outer margin of the central Flowers River pluton. Outcrops of fine-grained porphyritic granite are exposed along the southern caldera margin and in incised valleys within the caldera. Petrographic differences between granite within the caldera and nearer the limits of the

https://doi.org/10.1017/S0016756821000388 Published online by Cambridge University Press

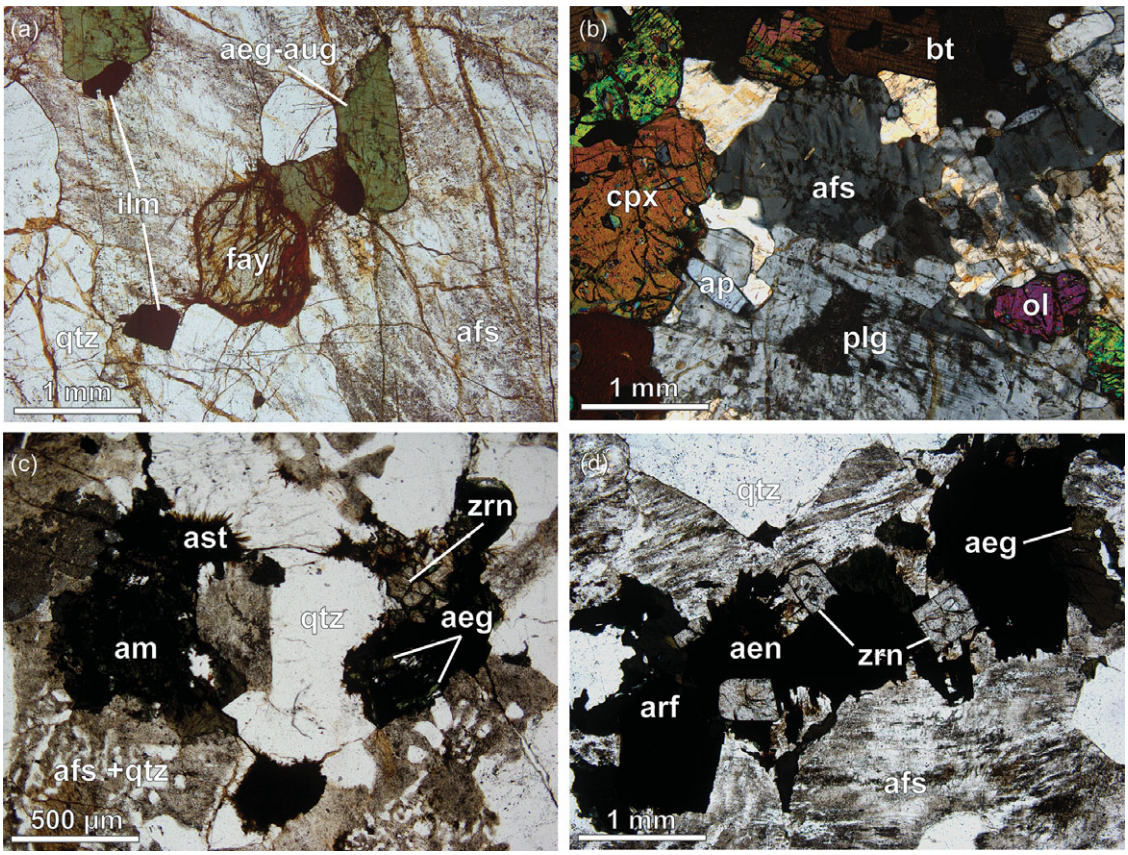


**Fig. 3.** (Colour online) Representative photomicrographs of intrusive lithologies from the Flowers River area. (a) Fayalitic olivine and (aegirine-)augite in a Three Bays Pluton fayalite granite. Plane-polarized light. (b) Representative mineralogy from a sample of moderately alkalic ferromonzogabbro (ferrodiorite). Cross-polarized light. (c) Alkali ferromagnesian minerals in a porphyritic Flowers River peralkaline granite. Note the graphic intergrowths of quartz and alkali feldspar. Plane-polarized light. (d) Alkali ferromagnesian and accessory minerals in an equigranular Flowers River peralkaline granite. Arfvedsonite and aenigmatite grow around large zircon inclusions within coarsely perthitic alkali feldspar. Plane-polarized light. Mineral abbreviations: aeg – aegirine; aeg-aug – aegirine-augite; aen – aenigmatite; afs – alkali feldspar; am – amphibole; ap – apatite; arf – arfvedsonite; bt – biotite; cpx – clinopyroxene; fay – fayalite; ilm – ilmenite; ol – olivine; plg – plagioclase; qtz – quartz; zrn – zircon.

central pluton are apparent in thin-section. Ferromagnesian and accessory mineral phases found near pluton margins are more coarse-grained and less altered, with Fe-oxide minerals present in considerable abundance. By contrast, the granite exposed within the caldera has developed much finer, hydrothermally altered interstitial ferromagnesian minerals and clusters of partially dissolved and/or recrystallized accessory phases (Fig. 3c). The essential mineralogical constituents in all samples are perthitic alkali feldspar, quartz, ferro-richteritic amphibole, aegirine-augite and zircon; primary aenigmatite was observed only in extracaldera granite, and feldspar in these rocks shows coarser perthitic lamellae (Fig. 3d). Ilmenite is the primary Fe–Ti oxide phase, rarely co-occurring with magnetite, and is typically observed reacting with rims of sodic-calcic amphibole to form aenigmatite. It is notable that diagnostic alkali minerals, following Le Maitre *et al.* (2005) (i.e. arfvedsonite, aegirine-augite and aenigmatite), only rarely display a conclusively magmatic appearance. Aegirine-augite, in particular, is typically present as metasomatic overgrowths on sodic-calcic amphiboles or as larger inclusion-rich crystals, although definitive magmatic specimens of both aegirine-augite and aenigmatite are present in some of the extracaldera peralkaline granite samples. The apparently secondary appearance of these phases in peralkaline granite from within the caldera may simply reflect a greater degree of interaction with late-magmatic volatiles. This is consistent with textural criteria in these samples indicating pervasive subsolidus re-equilibration, and with the behaviour of alkali phases during the late-stage petrogenesis of other peralkaline granite intrusions (e.g. Vasyukova & Williams-Jones, 2014; Yang *et al.* 2020).

Equigranular Flowers River Granite samples are A-type (Fig. 4), strongly ferroan (Fig. 5a), and plot in the $A_2$ field of Eby (1992); however, the three porphyritic samples plot within the $A_1$ field (Fig. 5b). Flowers River peralkaline granite (Table 2) shows geochemical profiles identical to the Three Bays granitoids, but appears more strongly differentiated (Fig. 6). Their major-element make-up includes slight elevations in $FeO_T$, $Na_2O$ and $K_2O$, and slightly greater depletion of CaO, MgO and $TiO_2$ compared with fayalite granite. Trace-element profiles similarly resemble the TBP granitoids, with the Flowers River Granite showing even more pronounced depletions in Ba, Sr and P, stronger negative Eu anomalies ($Eu/Eu^* = 0.13–0.19$) and greater absolute enrichment in all incompatible elements.

### 4.c. Nuiklavik Volcanics

A wide variety of lithofacies have been reported in the Nuiklavik caldera. A full discussion of the caldera's architecture is beyond the scope of this study; a more comprehensive assessment of structural and geochemical aspects of the volcanic succession can be found in CA White (unpub. PhD thesis, Memorial University of

https://doi.org/10.1017/S0016756821000388 Published online by Cambridge University Press

**Table 1.** Whole-rock major- and trace-element analyses for Three Bays Pluton lithologies

| | Granite | | | | Monzonite | | Anorthosite and ferrogabbro | | | Subsolvus granite | |
|---|---|---|---|---|---|---|---|---|---|---|---|
| Sample no. (wt%) | T0001 | T0003 | T0010 | T0015 | T0038 | T0045 | T0002 | T0121 | T0127 | T0105 | T0132 |
| $SiO_2$ | 73.40 | 66.83 | 72.38 | 74.03 | 59.83 | 56.12 | 51.36 | 51.94 | 48.08 | 74.89 | 73.54 |
| $Al_2O_3$ | 11.59 | 13.69 | 11.99 | 11.14 | 14.43 | 14.45 | 21.01 | 21.60 | 12.74 | 13.59 | 12.38 |
| $Fe_2O_3$ (T) | 3.89 | 7.05 | 3.75 | 4.28 | 8.50 | 10.91 | 6.62 | 6.19 | 17.63 | 1.28 | 2.85 |
| MnO | 0.075 | 0.115 | 0.072 | 0.064 | 0.145 | 0.207 | 0.072 | 0.064 | 0.218 | 0.020 | 0.040 |
| MgO | 0.09 | 0.17 | 0.12 | 0.12 | 1.65 | 1.74 | 0.83 | 1.39 | 3.44 | 0.29 | 0.40 |
| CaO | 0.48 | 1.91 | 0.47 | 0.66 | 3.97 | 4.18 | 7.86 | 8.46 | 6.70 | 0.55 | 1.13 |
| $Na_2O$ | 3.67 | 4.43 | 3.91 | 3.83 | 4.91 | 4.69 | 4.91 | 4.55 | 4.13 | 3.23 | 4.20 |
| $K_2O$ | 4.75 | 4.79 | 4.87 | 4.78 | 3.62 | 3.77 | 1.44 | 1.43 | 2.34 | 5.94 | 4.03 |
| $TiO_2$ | 0.362 | 0.636 | 0.355 | 0.420 | 1.405 | 1.652 | 1.524 | 1.322 | 3.380 | 0.126 | 0.361 |
| $P_2O_5$ | 0.04 | 0.10 | 0.03 | 0.05 | 0.65 | 0.73 | 0.40 | 0.55 | 2.03 | 0.04 | 0.07 |
| LOI | 0.40 | 0.49 | 1.89 | 0.29 | 1.02 | 0.62 | 2.31 | 3.05 | −0.28 | 0.60 | 0.38 |
| Total | 98.76 | 100.2 | 99.83 | 99.68 | 100.1 | 99.06 | 98.34 | 100.6 | 100.4 | 100.6 | 99.39 |
| Zn (ppm) | 100 | 150 | 110 | 130 | 140 | 370 | 60 | 50 | 160 | < 30 | 80 |
| Ga | 26 | 29 | 27 | 28 | 36 | 35 | 24 | 20 | 21 | 16 | 20 |
| Ge | 1.7 | 1.7 | 1.5 | 1.5 | 1.9 | 2.3 | 1.2 | 1.0 | 1.8 | 0.9 | 1.2 |
| Rb | 136 | 132 | 147 | 163 | 85 | 129 | 22 | 88 | 62 | 165 | 102 |
| Sr | 25 | 99 | 29 | 26 | 130 | 144 | 421 | 462 | 203 | 188 | 414 |
| Y | 79.8 | 70.3 | 89.7 | 63.8 | 83.4 | 252.0 | 21.2 | 27.1 | 69.1 | 5.6 | 36.3 |
| Zr | 652 | 594 | 661 | 729 | 1129 | 1364 | 229 | 178 | 428 | 137 | 613 |
| Nb | 38.2 | 35.9 | 34.1 | 36.9 | 46.2 | 139.0 | 8.4 | 10.0 | 30.6 | 1.9 | 22.8 |
| Ba | 399 | 1257 | 449 | 258 | 440 | 568 | 779 | 590 | 1032 | 1105 | 3016 |
| Nb | 38.2 | 35.9 | 34.1 | 36.9 | 46.2 | 139.0 | 8.4 | 10.0 | 30.6 | 1.9 | 22.8 |
| Sn | 5 | 5 | 5 | 6 | 8 | 25 | 2 | 6 | 4 | 1 | 2 |
| La | 186 | 101 | 208 | 133 | 294 | 406 | 33 | 32 | 80 | 74 | 142 |
| Ce | 370 | 204 | 376 | 255 | 545 | 782 | 65.8 | 63.6 | 176 | 131 | 274 |
| Pr | 36.5 | 23.1 | 39.1 | 26.7 | 55.3 | 81.8 | 7.3 | 7.5 | 21.4 | 13.3 | 27.2 |
| Nd | 117 | 86 | 127 | 92 | 189 | 276 | 28 | 30 | 86 | 40 | 91 |
| Sm | 18.5 | 15.8 | 19.6 | 15.0 | 26.4 | 44.0 | 5.41 | 5.47 | 16.4 | 4.93 | 12.1 |
| Eu | 1.23 | 2.72 | 1.43 | 0.97 | 3.22 | 4.36 | 2.85 | 1.82 | 3.46 | 0.59 | 2.44 |
| Gd | 13.8 | 13.7 | 15.3 | 11.9 | 18.4 | 36.7 | 4.65 | 5.00 | 14.9 | 2.53 | 8.51 |
| Tb | 2.32 | 2.13 | 2.58 | 1.92 | 2.71 | 6.42 | 0.68 | 0.82 | 2.16 | 0.25 | 1.20 |
| Dy | 14.4 | 12.9 | 15.4 | 11.5 | 15.6 | 41.5 | 3.99 | 4.65 | 12.7 | 1.15 | 6.87 |
| Ho | 3.01 | 2.55 | 3.21 | 2.33 | 3.00 | 8.87 | 0.79 | 0.92 | 2.60 | 0.20 | 1.37 |
| Er | 9.07 | 7.54 | 9.34 | 7.07 | 9.05 | 27.6 | 2.32 | 2.57 | 7.13 | 0.58 | 3.99 |
| Tm | 1.39 | 1.11 | 1.43 | 1.08 | 1.38 | 4.26 | 0.31 | 0.36 | 1.00 | 0.08 | 0.59 |
| Yb | 9.28 | 7.44 | 9.27 | 7.81 | 9.13 | 28.8 | 2.1 | 2.23 | 6.46 | 0.49 | 4.05 |
| Lu | 1.41 | 1.15 | 1.42 | 1.23 | 1.55 | 4.32 | 0.34 | 0.34 | 1.01 | 0.08 | 0.64 |
| Hf | 15.5 | 13.7 | 12.7 | 15.0 | 24.5 | 43.2 | 5.30 | 3.80 | 8.60 | 3.90 | 13.3 |
| Ta | 2.50 | 2.28 | 2.46 | 2.79 | 2.87 | 9.15 | 0.55 | 0.59 | 1.88 | 0.16 | 1.29 |
| Pb | 21 | 26 | 19 | 14 | 21 | 95 | 7 | 12 | 20 | 24 | 20 |
| Th | 19.8 | 14.7 | 18.5 | 15.2 | 17.9 | 45.2 | 3.02 | 2.17 | 6.52 | 24.5 | 13.3 |
| U | 1.67 | 2.11 | 1.50 | 2.44 | 2.38 | 4.57 | 0.50 | 0.37 | 1.18 | 1.28 | 0.88 |
| AI | 0.96 | 0.91 | 0.98 | 1.03 | 0.83 | 0.82 | 0.46 | 0.42 | 0.73 | 0.86 | 0.91 |
| A/CNK | 0.96 | 0.86 | 0.95 | 0.88 | 0.75 | 0.74 | 0.88 | 0.88 | 0.59 | 1.07 | 0.93 |
| Fe* | 0.908 | 0.904 | 0.876 | 0.890 | 0.539 | 0.587 | 0.644 | 0.503 | 0.538 | 0.501 | 0.618 |
| Th/U | 11.9 | 6.97 | 12.3 | 6.23 | 7.52 | 9.89 | 6.04 | 5.86 | 5.53 | 19.1 | 15.1 |
| 10 000×Ga/Al | 4.24 | 4.00 | 4.26 | 4.75 | 4.71 | 4.58 | 2.16 | 1.75 | 3.12 | 2.23 | 3.05 |
| Eu/Eu* | 0.22 | 0.55 | 0.24 | 0.21 | 0.42 | 0.32 | 1.69 | 1.04 | 0.66 | 0.45 | 0.70 |

https://doi.org/10.1017/S0016756821000388 Published online by Cambridge University Press

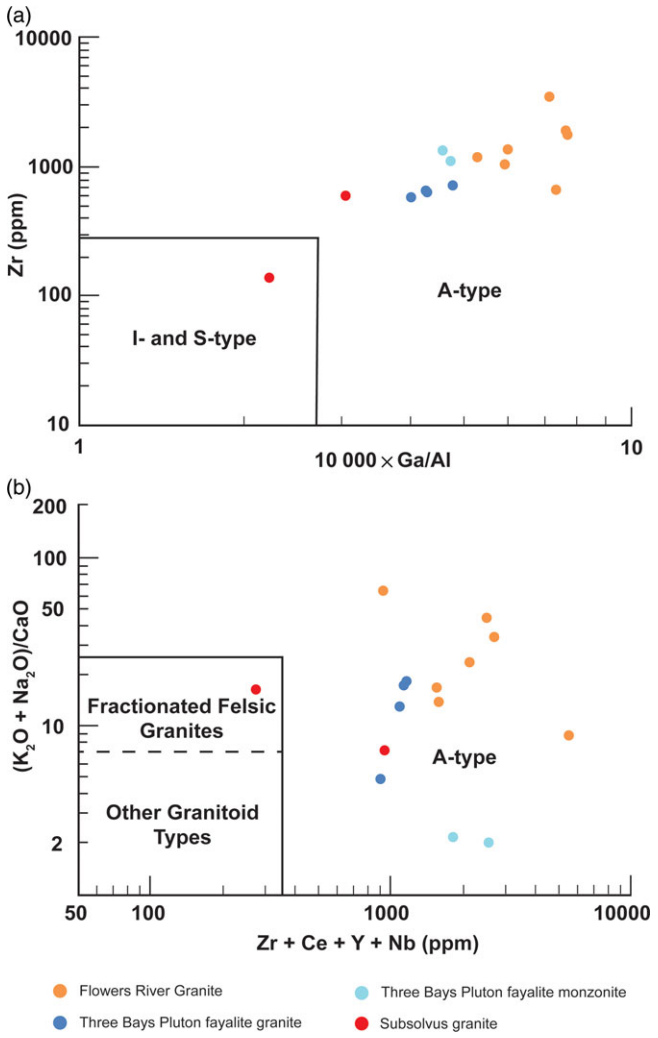


**Fig. 4.** (Colour online) (a) Zr versus 10 000 × Al/Ga and (b) $(K_2O+Na_2O)/CaO$ versus Zr + Ce + Y + Nb diagrams after Whalen *et al.* (1987). All samples plot in the A-type field except for one sample of subsolvus granite.

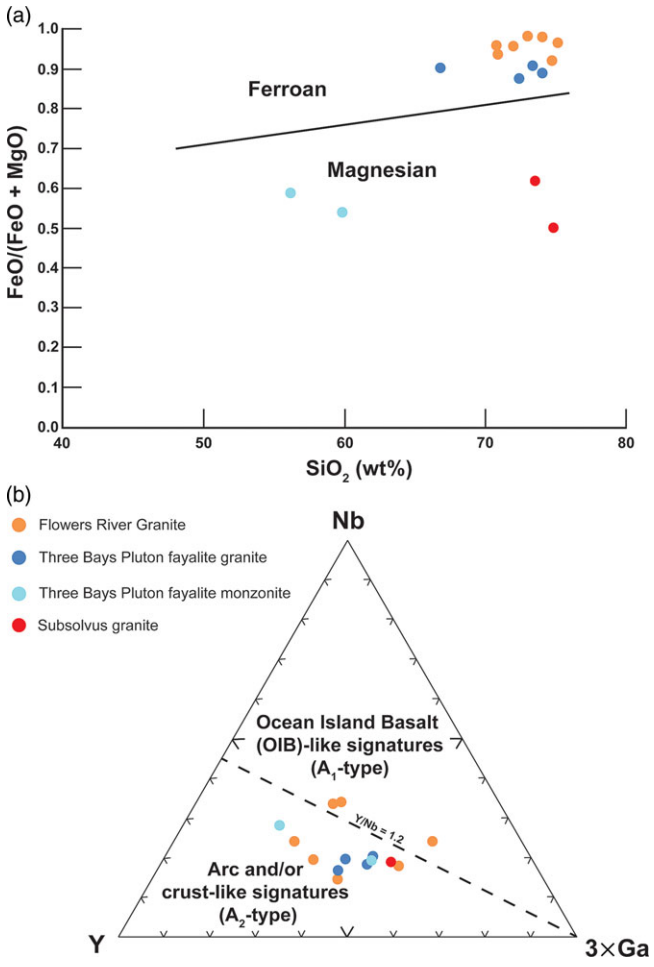


**Fig. 5.** (Colour online) (a) FeO/(FeO+MgO) versus $SiO_2$ plot after Frost & Frost (2008*a*). Samples of Flowers River Granite and Three Bays Pluton fayalite granite are ferroan, whereas monzonite and subsolvus granite plot in the sub-ferroan (magnesian) field. (b) Y versus Nb versus 3×Ga ternary plot after Eby (1992) for samples that plot as A-type in Figure 3. Most samples plot in the $A_2$ field, but three porphyritic peralkaline granite samples have Y/Nb < 1.2 and accordingly plot in the $A_1$ field.

Newfoundland, 1980) and Miller (1993). Previous researchers have generally agreed that the Nuiklavik Volcanics are largely composed of volcaniclastic rocks; however, intensity of alteration, limited cross-sectional exposure, and the massive nature of certain samples often prohibited conclusive identification of a particular volcanic mode of emplacement for this study. The Nuiklavik rocks encountered in this study can broadly be divided into aphyric (Table 3) and porphyritic varieties (Table 4), and textural evidence is generally consistent with these rocks being volcaniclastic in nature. Phenocryst assemblages in porphyritic facies almost exclusively comprise quartz and Carlsbad twinned, microperthitic to unexsolved alkali feldspar. More rarely, larger (< 2 mm) polycrystalline lithic fragments of plagioclase and K-feldspar co-occur with smaller quartz phenocrysts in lithic tuffs. Aphyric rocks encountered over the course of this study commonly preserve discontinuous flow folia or relict fiamme, supporting earlier suggestions that welded tuffs constitute a large proportion of the Nuiklavik Volcanics (Kerr, 2011). Well-preserved devitrification textures, including micropoikilitic quartz and spherulites, indicate that many specimens were initially composed almost entirely of glass. Lithophysae are common in aphyric facies, and are commonly filled with a hydrothermal assemblage of quartz, Fe–Ti oxides, fluorite and sphalerite (Fig. 7a).

The Nuiklavik rocks show by far the widest variability in the extent and style of alteration of any unit encountered in the study area, and this is reflected in their geochemistry (Fig. 6). This manifests primarily in their highly variable degrees of enrichment and/or depletion, as their trace-element profiles generally do not deviate considerably from those of the Flowers River and Nain suites. Incompatible element signatures in Nuiklavik rocks can show either more or less absolute enrichment compared with their intrusive counterparts. In particular, the degree of HREE enrichment varies widely, with $(La/Lu)_{CN}$ between 1.04 and 12.2. There is no similar compositional breadth in the depleted elements (e.g. Ba and Sr), and Eu anomalies in the Nuiklavik rocks occupy a narrow range of values ($Eu/Eu^* = 0.10–0.19$). A systematic correlation exists between greater absolute REE concentrations and higher modal abundances of secondary bastnäsite-(Ce) and monazite-(Ce) and intensity of alteration within a sample, suggesting the enrichment is metasomatic in nature. Densely disseminated submicroscopic zircon appears to be the primary controller of these elements in samples showing the most elevated HREE concentrations.

https://doi.org/10.1017/S0016756821000388 Published online by Cambridge University Press

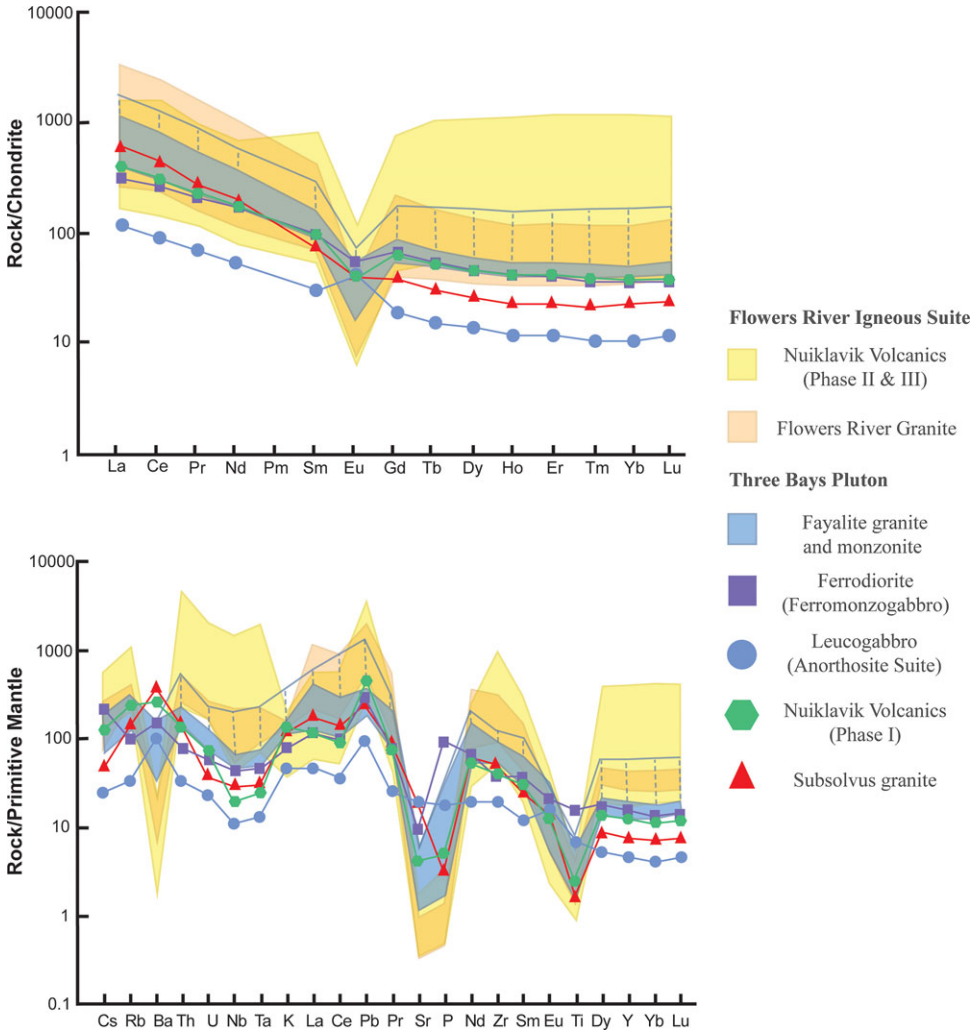


**Fig. 6.** (Colour online) Chondrite-normalized REE (top) and primitive-mantle-normalized trace-element (bottom) diagrams for the various suites of rocks exposed in the vicinity of the Flowers River Igneous Suite. Compositional ranges are provided for highly represented suites. The compositional profile of one enriched sample of fayalite monzonite (CXAT0045) is connected by dashed line to the more typical compositional range for this suite. Values plotted for the Nuiklavik Volcanics (Phase I) are an average of two samples. Normalization factors after Sun & McDonough (1989).

Three distinct alteration styles are observed within the caldera, and can be defined by the dominant groundmass minerals. White mica is the most widespread style of alteration, and fine-grained micaceous masses commonly encroach on feldspar phenocrysts or pseudomorph them entirely (Fig. 7b). A second, distinct hematitic alteration imparts a red to dark brown colour on the groundmass, and red disseminated hematite particles cloud feldspar phenocrysts in affected rocks (Fig. 7c). Notably, this is the only alteration style accompanied by graphic textured pyroclasts of possible juvenile or accidental origin. Finally, a chlorite-dominant alteration was observed in two samples from the SW of the caldera (Fig. 7d), although chloritic alteration frequently occurs with bastnäsite-(Ce) and monazite-(Ce) in otherwise sericitized rocks. Alteration styles in very fine-grained, aphyric ash-flows are more difficult to assess, but EDS results indicate an assemblage comprising predominantly chlorite and quartz.

Samples affected by the chlorite-dominant alteration seen in the SW of the caldera diverge from the geochemical trends common among the other volcanic lithologies. These samples are less strongly depleted in Sr and P than other volcanics, show a marked Nb–Ta trough and are enriched in Ba (Fig. 6). They are also the only volcanic lithologies observed to contain plagioclase, which is present with K-feldspar in polycrystalline lapilli (Fig. 7d). Although accidental fragments of monzonite could serve to impart moderately elevated Sr and Ba relative to the wholesale depletion observed throughout the caldera, imparting Ba concentrations in excess of the monzonite itself is less plausible. Furthermore, only one of the two samples contains plagioclase-bearing lithic fragments, despite sharing near-identical geochemical signatures. Accordingly, these mineralogical and geochemical characteristics are deemed primary geochemical features of the samples. Along with geochronological constraints discussed in Sections 5.c and 6.b, these geochemically distinct lithologies are referred to here as Phase I of the Nuiklavik Volcanics; volcanic lithologies whose geochemistry more closely resembles that of the Flowers River Granite are grouped into Phase II and Phase III (Fig. 6; see discussion in Section 6.b).

### *4.d. Subsolvus granite*

Two outcrops of subsolvus granite were encountered over the course of mapping. One of these exposures was along the eastern edge of the Nuiklavik caldera, and was mapped previously as belonging to the

https://doi.org/10.1017/S0016756821000388 Published online by Cambridge University Press

**Table 2.** Whole-rock major- and trace-element analyses for the Flowers River peralkaline granite. ND – not determined.

| Sample no. (wt%) | T0004 | T0008 | T0016 | T0029 | T0030 | T0126 | T0136 |
|---|---|---|---|---|---|---|---|
| $SiO_2$ | 70.94 | 70.81 | 75.21 | 73.03 | 74.07 | 72.04 | 74.80 |
| $Al_2O_3$ | 11.86 | 11.69 | 11.64 | 11.60 | 11.15 | 9.02 | 11.10 |
| $Fe_2O_3$ (T) | 5.17 | 5.01 | 3.82 | 4.86 | 4.69 | 7.89 | 4.10 |
| MnO | 0.069 | 0.056 | 0.053 | 0.076 | 0.088 | 0.102 | 0.043 |
| MgO | 0.08 | 0.05 | 0.03 | 0.02 | 0.02 | 0.08 | 0.08 |
| CaO | 0.67 | 0.40 | 0.14 | 0.28 | 0.20 | 0.85 | 0.49 |
| $Na_2O$ | 4.38 | 4.51 | 3.90 | 4.66 | 4.05 | 3.43 | 3.78 |
| $K_2O$ | 4.95 | 4.99 | 4.99 | 4.79 | 4.72 | 3.98 | 4.42 |
| $TiO_2$ | 0.411 | 0.288 | 0.315 | 0.320 | 0.309 | 0.929 | 0.550 |
| $P_2O_5$ | 0.03 | 0.01 | ND | ND | 0.01 | 0.02 | 0.04 |
| LOI | 0.21 | 0.52 | 0.67 | 0.48 | 0.59 | −0.06 | 0.18 |
| Total | 98.76 | 98.33 | 100.8 | 100.1 | 99.91 | 98.28 | 99.59 |
| Zn (ppm) | 200 | 140 | 150 | 210 | 260 | 320 | 130 |
| Ga | 37 | 37 | 45 | 47 | 45 | 34 | 31 |
| Ge | 2.0 | 1.9 | 1.6 | 2.3 | 2.2 | 3.2 | 1.5 |
| Rb | 205 | 262 | 207 | 242 | 228 | 254 | 150 |
| Sr | 17 | 18 | 9 | 13 | 7 | 20 | 32 |
| Y | 123 | 161 | 47 | 153 | 163 | 192 | 53 |
| Zr | 1050 | 1370 | 671 | 1825 | 1855 | 3544 | 1210 |
| Nb | 39.6 | 65.2 | 57.9 | 150 | 150 | 93.9 | 31.6 |
| Ba | 147 | 71 | 44 | 65 | 50 | 86 | 201 |
| Nb | 39.6 | 65.2 | 57.9 | 150 | 150 | 93.9 | 31.6 |
| Sn | 10 | 18 | 9 | 19 | 19 | 13 | 5 |
| La | 179 | 264 | 66.4 | 236 | 149 | 844 | 116 |
| Ce | 363 | 508 | 151 | 546 | 310 | 1620 | 248 |
| Pr | 41.2 | 52.4 | 16.1 | 51.1 | 31.9 | 155 | 25.5 |
| Nd | 152 | 173 | 55.5 | 169 | 106 | 506 | 90.0 |
| Sm | 27.7 | 28.6 | 11.1 | 31.7 | 20.1 | 66.6 | 14.9 |
| Eu | 1.390 | 1.270 | 0.473 | 1.400 | 0.887 | 2.400 | 0.839 |
| Gd | 23.7 | 23.7 | 8.71 | 25.4 | 17.9 | 44.7 | 11.7 |
| Tb | 3.80 | 4.16 | 1.51 | 4.41 | 3.74 | 6.24 | 1.81 |
| Dy | 22.3 | 25.8 | 9.18 | 27.4 | 27.5 | 35.4 | 10.3 |
| Ho | 4.54 | 5.64 | 1.87 | 5.74 | 6.24 | 6.95 | 2.04 |
| Er | 13.4 | 17.4 | 6.09 | 18.0 | 19.6 | 21.1 | 5.87 |
| Tm | 1.92 | 2.75 | 0.99 | 2.81 | 3.04 | 3.11 | 0.88 |
| Yb | 13.0 | 18.4 | 7.83 | 19.1 | 20.5 | 20.9 | 6.08 |
| Lu | 2.00 | 2.88 | 1.40 | 3.07 | 3.20 | 3.40 | 0.99 |
| Hf | 24.1 | 32.0 | 17.1 | 46.1 | 47.8 | 63.8 | 21.8 |
| Ta | 3.65 | 6.48 | 4.15 | 8.45 | 8.99 | 6.38 | 1.77 |
| Pb | 43 | 143 | 21 | 45 | 38 | 63 | 19 |
| Th | 22.6 | 26.6 | 12.6 | 27.2 | 26.1 | 45.6 | 9.8 |
| U | 3.66 | 4.58 | 1.71 | 5.25 | 4.50 | 5.68 | 1.18 |
| AI | 1.06 | 1.10 | 1.02 | 1.11 | 1.06 | 1.10 | 0.99 |
| A/CNK | 0.86 | 0.86 | 0.96 | 0.87 | 0.92 | 0.78 | 0.93 |
| Fe* | 0.936 | 0.958 | 0.967 | 0.982 | 0.982 | 0.957 | 0.921 |
| Th/U | 6.17 | 5.81 | 7.37 | 5.18 | 5.80 | 8.03 | 8.31 |
| 10 000×Ga/Al | 5.89 | 5.98 | 7.31 | 7.66 | 7.63 | 7.12 | 5.28 |
| Eu/Eu* | 0.16 | 0.14 | 0.14 | 0.15 | 0.14 | 0.13 | 0.19 |

https://doi.org/10.1017/S0016756821000388 Published online by Cambridge University Press

**Table 3.** Whole-rock major- and trace-element analyses for aphyric facies of the Nuiklavik Volcanics.

| Sample no. (wt%) | T0022A | T0022C | T0025 | T0042 | T0116 | T0117 | T0119 |
|---|---|---|---|---|---|---|---|
| $SiO_2$ | 74.87 | 73.97 | 75.91 | 75.78 | 80.07 | 71.67 | 68.53 |
| $Al_2O_3$ | 9.70 | 9.45 | 9.36 | 9.10 | 7.99 | 8.57 | 16.1 |
| $Fe_2O_3$ (T) | 6.42 | 6.81 | 7.53 | 5.79 | 6.48 | 13.4 | 2.70 |
| MnO | 0.055 | 0.081 | 0.096 | 0.043 | 0.059 | 0.114 | 0.063 |
| MgO | 0.05 | 0.04 | 0.07 | 0.09 | 0.03 | 0.07 | 0.04 |
| CaO | 0.31 | 0.16 | 0.12 | 0.19 | 0.04 | 0.05 | 0.07 |
| $Na_2O$ | 2.80 | 3.66 | 0.08 | 0.32 | 0.11 | 0.07 | 0.19 |
| $K_2O$ | 4.41 | 4.50 | 4.54 | 5.80 | 1.71 | 1.07 | 4.57 |
| $TiO_2$ | 0.226 | 0.224 | 0.247 | 0.347 | 0.376 | 0.363 | 0.878 |
| $P_2O_5$ | N.D. | 0.02 | 0.01 | 0.02 | 0.05 | 0.03 | 0.07 |
| LOI | 0.35 | 0.20 | 1.42 | 0.36 | 1.91 | 2.28 | 2.80 |
| Total | 99.19 | 99.11 | 99.39 | 97.85 | 98.83 | 97.69 | 96.02 |
| Zn (ppm) | 520 | 520 | 530 | 560 | 1300 | 550 | 360 |
| Ga | 44 | 43 | 40 | 29 | 40 | 41 | 75 |
| Ge | 2.2 | 3.6 | 1.3 | 1.2 | 1.7 | 1.6 | 1.7 |
| Rb | 521 | 520 | 504 | 353 | 253 | 191 | 584 |
| Sr | 12 | 13 | 11 | 34 | 8 | 7 | 15 |
| Y | 480 | 465 | 505 | 433 | 973 | 889 | 1720 |
| Zr | 4584 | 4558 | 4593 | 3778 | 8735 | 7147 | > 10 000 |
| Nb | 270 | 260 | 221 | 131 | 549 | 412 | 975 |
| Ba | 17 | 19 | 47 | 114 | 29 | 50 | 50 |
| Sn | 48 | 52 | 51 | 26 | 114 | 102 | 205 |
| La | 353 | 334 | 373 | 290 | 764 | 192 | 284 |
| Ce | 770 | 729 | 808 | 629 | 1700 | 474 | 938 |
| Pr | 85.1 | 80.9 | 90.9 | 71.8 | 181 | 51.8 | 73.7 |
| Nd | 301 | 285 | 316 | 270 | 628 | 206 | 314 |
| Sm | 66.0 | 64.0 | 71.3 | 56.8 | 137 | 74.2 | 123 |
| Eu | 2.21 | 2.29 | 2.40 | 2.40 | 6.08 | 4.07 | 6.93 |
| Gd | 64.1 | 64.3 | 68.2 | 56.1 | 130 | 87.5 | 157 |
| Tb | 12.2 | 12.1 | 12.8 | 10.7 | 24.6 | 19.3 | 37.3 |
| Dy | 79.1 | 78.1 | 85.9 | 71.2 | 162 | 140 | 269 |
| Ho | 16.9 | 16.3 | 18.0 | 15.4 | 34.1 | 32.1 | 60.6 |
| Er | 52.1 | 49.9 | 55.4 | 46.6 | 105 | 104 | 188 |
| Tm | 7.84 | 7.59 | 8.43 | 7.03 | 15.9 | 16.0 | 29.6 |
| Yb | 51.5 | 49.9 | 55.5 | 43.3 | 103 | 105 | 195 |
| Lu | 7.72 | 7.44 | 7.89 | 6.47 | 15.1 | 15.4 | 28.3 |
| Hf | 111 | 109 | 108 | 98.4 | 227 | 160 | 483 |
| Ta | 21.4 | 20.6 | 20.6 | 11.0 | 43.8 | 36.9 | 76.3 |
| Pb | 138 | 153 | 157 | 127 | 290 | 237 | 75 |
| Bi | 0.4 | 0.4 | 0.3 | 0.2 | 0.4 | 0.2 | 0.2 |
| Th | 91.4 | 86.8 | 95.7 | 78.0 | 208 | 178 | 372 |
| U | 15.9 | 15.8 | 17.3 | 9.79 | 36.4 | 36.6 | 42.0 |
| AI | 0.97 | 1.15 | 0.54 | 0.75 | 0.25 | 0.15 | 0.33 |
| A/CNK | 0.98 | 0.85 | 1.78 | 1.27 | 3.80 | 6.28 | 2.99 |
| Fe* | 0.967 | 0.975 | 0.961 | 0.936 | 0.980 | 0.978 | 0.939 |
| Th/U | 5.75 | 5.49 | 5.53 | 7.97 | 5.71 | 4.86 | 8.86 |
| 10 000×Ga/Al | 8.57 | 8.60 | 8.08 | 6.02 | 9.46 | 9.04 | 8.80 |
| Eu/Eu* | 0.10 | 0.11 | 0.10 | 0.13 | 0.14 | 0.15 | 0.15 |

https://doi.org/10.1017/S0016756821000388 Published online by Cambridge University Press

**Table 4.** Whole-rock major- and trace-element analyses for porphyritic facies of the Nuiklavik Volcanics. ND – not determined.

| Sample no. (wt%) | T0009A | T0009B | T0014 | T0018 | T0026A | T0026B | T0046 | T0048 | T0084 | T0085 | T0094 |
|---|---|---|---|---|---|---|---|---|---|---|---|
| $SiO_2$ | 72.34 | 74.14 | 73.05 | 75.55 | 67.26 | 76.8 | 74.33 | 71.28 | 75.33 | 73.92 | 74.77 |
| $Al_2O_3$ | 11.30 | 11.35 | 9.59 | 10.50 | 22.01 | 14.00 | 11.53 | 12.65 | 10.86 | 12.89 | 10.69 |
| $Fe_2O_3$ (T) | 6.33 | 6.20 | 9.43 | 5.68 | 1.04 | 2.65 | 4.84 | 7.48 | 3.93 | 3.59 | 4.98 |
| MnO | 0.074 | 0.076 | 0.093 | 0.038 | 0.013 | 0.028 | 0.029 | 0.071 | 0.048 | 0.019 | 0.062 |
| MgO | 0.22 | 0.15 | 0.09 | 0.05 | 0.04 | 0.03 | 0.05 | 0.10 | 0.04 | 0.03 | 0.06 |
| CaO | 1.94 | 0.32 | 0.06 | 0.11 | 0.05 | 0.05 | 0.05 | 0.11 | 0.19 | 0.08 | 0.19 |
| $Na_2O$ | 1.49 | 0.15 | 1.90 | 1.24 | 0.46 | 0.20 | 0.19 | 0.13 | 4.22 | 4.91 | 2.95 |
| $K_2O$ | 4.39 | 4.66 | 4.50 | 5.44 | 5.62 | 3.54 | 5.56 | 3.77 | 4.44 | 3.87 | 4.55 |
| $TiO_2$ | 0.616 | 0.612 | 0.338 | 0.380 | 0.601 | 0.385 | 0.333 | 0.407 | 0.182 | 0.295 | 0.291 |
| $P_2O_5$ | 0.13 | 0.10 | ND | 0.02 | 0.06 | 0.02 | 0.01 | 0.05 | ND | 0.03 | ND |
| LOI | 0.96 | 1.23 | 0.88 | 0.86 | 3.15 | 2.29 | 1.49 | 2.32 | 0.32 | 0.40 | 1.15 |
| Total | 99.78 | 99.00 | 99.95 | 99.86 | 100.3 | 99.98 | 98.43 | 98.37 | 99.56 | 100.0 | 99.7 |
| Zn (ppm) | 130 | 120 | 100 | 300 | 30 | 80 | 60 | 120 | 540 | 70 | 170 |
| Ga | 25 | 21 | 40 | 35 | 73 | 55 | 33 | 35 | 45 | 35 | 34 |
| Ge | 1.1 | 0.8 | 2.2 | 1.8 | 1.1 | 1.3 | 1 | 1.2 | 2.6 | 1.7 | 2 |
| Rb | 147 | 207 | 374 | 452 | 661 | 381 | 279 | 241 | 531 | 197 | 289 |
| Sr | 173 | 54 | 11 | 14 | 20 | 9 | 15 | 10 | 10 | 11 | 11 |
| Y | 66.4 | 61.5 | 372 | 274 | 196 | 482 | 115 | 126 | 339 | 129 | 133 |
| Zr | 556 | 519 | 3958 | 2790 | 2209 | 5240 | 1022 | 1215 | 2034 | 1179 | 1687 |
| Nb | 16.1 | 14.3 | 180 | 171 | 135 | 291 | 51.3 | 55.3 | 197 | 78.1 | 93.5 |
| Ba | 2132 | 1920 | 35 | 43 | 130 | 49 | 142 | 54 | 12 | 88 | 52 |
| Sn | 3 | 3 | 24 | 30 | 20 | 62 | 15 | 11 | 49 | 13 | 15 |
| La | 96.8 | 93.1 | 316 | 268 | 297 | 265 | 176 | 255 | 141 | 126 | 183 |
| Ce | 196 | 191 | 683 | 454 | 540 | 579 | 347 | 493 | 291 | 180 | 374 |
| Pr | 22.5 | 21.7 | 75.6 | 59.8 | 65.6 | 65.2 | 37.3 | 51.7 | 33.2 | 30.5 | 40.1 |
| Nd | 83.8 | 81.8 | 258 | 207 | 227 | 232 | 125 | 174 | 111 | 102 | 139 |
| Sm | 15.3 | 15.3 | 51.4 | 40.2 | 39.3 | 56.1 | 21.2 | 28.6 | 27.5 | 20.0 | 26.0 |
| Eu | 2.32 | 2.52 | 2.05 | 1.83 | 1.58 | 2.23 | 0.98 | 1.39 | 0.70 | 0.88 | 0.98 |
| Gd | 13.2 | 12.7 | 48.5 | 37.8 | 31.8 | 56.6 | 17.7 | 23.0 | 28.6 | 18.4 | 22.1 |
| Tb | 2.02 | 1.94 | 9.54 | 6.91 | 5.27 | 11.7 | 3.09 | 3.69 | 6.28 | 3.38 | 4.01 |
| Dy | 11.9 | 11.5 | 63.2 | 44.6 | 33.7 | 77.4 | 20.0 | 21.6 | 45.7 | 21.3 | 25.5 |
| Ho | 2.42 | 2.26 | 13.5 | 9.39 | 7.01 | 16.7 | 4.17 | 4.51 | 10.6 | 4.59 | 5.21 |
| Er | 7.06 | 6.58 | 42.4 | 28.5 | 21.6 | 50.9 | 12.7 | 13.7 | 35.0 | 13.5 | 16.1 |
| Tm | 1.01 | 0.95 | 6.37 | 4.21 | 3.09 | 7.73 | 1.98 | 2.05 | 5.82 | 2.06 | 2.62 |
| Yb | 6.41 | 6.16 | 41.2 | 27.3 | 21.0 | 50.4 | 12.9 | 13.4 | 39.0 | 13.9 | 18.1 |
| Lu | 1.00 | 0.96 | 6.40 | 4.28 | 3.25 | 7.55 | 1.97 | 2.16 | 5.72 | 2.11 | 2.82 |
| Hf | 14.2 | 13.7 | 85.2 | 68.0 | 51.9 | 125 | 24.3 | 26.7 | 59.6 | 28.2 | 39.7 |
| Ta | 1.15 | 1.13 | 14.0 | 12.5 | 7.27 | 19.7 | 4.35 | 4.52 | 20.4 | 6.04 | 7.27 |
| Pb | 36 | 37 | 70 | 69 | 84 | 116 | 47 | 23 | 112 | 38 | 24 |
| Bi | 0.2 | 0.1 | 0.2 | 0.1 | 0.1 | 0.2 | 0.1 | 0.1 | 0.2 | < 0.1 | < 0.1 |
| Th | 13.8 | 12.8 | 66.7 | 54.8 | 35.5 | 86.7 | 22.6 | 23.4 | 60.4 | 24.0 | 36 |
| U | 1.73 | 1.85 | 9.89 | 7.95 | 6.03 | 16.7 | 3.40 | 4.22 | 12.0 | 2.3 | 3.64 |
| Al | 0.64 | 0.47 | 0.83 | 0.76 | 0.31 | 0.30 | 0.55 | 0.34 | 1.08 | 0.95 | 0.91 |
| A/CNK | 1.05 | 1.93 | 1.18 | 1.29 | 3.18 | 3.29 | 1.80 | 2.81 | 0.90 | 1.04 | 1.06 |
| Fe* | 0.867 | 0.904 | 0.960 | 0.963 | 0.855 | 0.953 | 0.956 | 0.944 | 0.957 | 0.965 | 0.950 |
| Th/U | 7.98 | 6.92 | 6.74 | 6.89 | 5.89 | 5.19 | 6.65 | 5.55 | 5.03 | 10.43 | 9.89 |
| 10 000×Ga/Al | 4.18 | 3.45 | 7.88 | 6.23 | 6.27 | 7.42 | 5.41 | 5.23 | 7.83 | 5.13 | 6.01 |
| Eu/Eu* | 0.49 | 0.54 | 0.12 | 0.14 | 0.13 | 0.12 | 0.15 | 0.16 | 0.08 | 0.14 | 0.12 |

https://doi.org/10.1017/S0016756821000388 Published online by Cambridge University Press

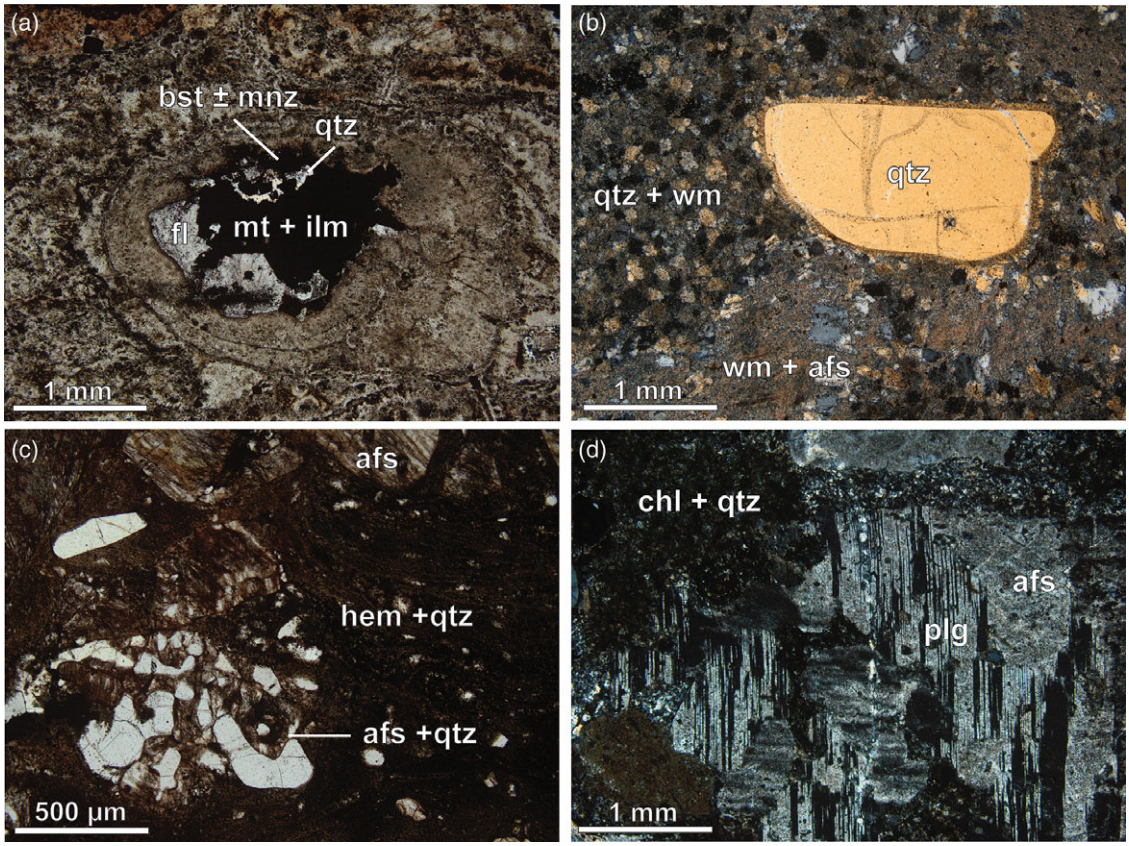


**Fig. 7.** (Colour online) Representative photomicrographs of volcanic lithologies from the Flowers River area. (a) Large polycrystalline lithic clast of plagioclase and alkali feldspar in a chlorite-altered lithic-rich volcanic sample from the southwestern region of the caldera. Cross-polarized light. (b) Graphic-textured pyroclast set in a flow-banded, hematized crystal tuff. Plane-polarized light. (c) Filled lithophysae within a hematized aphyric volcanic sample from the northwestern region of the caldera. Coarse eu- to subhedral fluorite and oxide minerals suggest secondary growth occurred within primary void space. Accessory REE-bearing minerals (bastnäsite-(Ce) and monazite-(Ce)) occur in subordinate quantities. Cross-polarized light. (d) Porphyritic white mica-altered sample. White mica alteration in the Nuiklavik caldera is commonly accompanied by groundmass textures defined by microperthitic quartz mosaics. Cross-polarized light. Mineral abbreviations: afs – alkali feldspar; bst – bastnäsite-(Ce); chl – chlorite; fl – fluorite; hem – hematite; ilm – ilmenite; mnz – monazite; mt – magnetite; plg – plagioclase; qtz – quartz; wm – white mica.

Three Bays Pluton (Hill, 1982). The other subsolvus granite is petrologically distinct and has a metaluminous to weakly peraluminous chemistry (A/CNK = 0.93–1.07; Table 1). Their trace-element profiles are distinct among the intrusive samples collected, showing comparative depletion in incompatible elements and weaker negative Eu anomalies (Eu/Eu* = 0.45–0.70), while being undepleted in Sr and Ba (Fig. 6). The rocks are dominated by coarse-grained quartz, plagioclase and unexsolved alkali feldspar in approximately equal proportions. Minor quantities (< 10 vol.%) of biotite and chlorite occur interstitial to these phases. Gneissic xenoliths up to 0.5 m in diameter were evident in outcrop, and microxenolith domains composed of biotite + quartz ± titanite are present in thin section. These domains are rimmed by overgrowths of green augite. The extent and style of subsolidus alteration present in the subsolvus granite is consistent with its previous inclusion with the other Three Bays Pluton granitoid lithologies, and this is further supported by geochronological data (see Section 5.d).

## 5. U–Pb geochronology

Zircon from 17 samples were analysed *in situ* using SEM backscatter-electron (SEM-BSE) images to inform spot placement and avoid mixed analyses of zircon age domains. Zircon U–Pb age results are summarized in Table 5. Data were pruned by progressive exclusion based on discordance estimates for each data point, with age concordance cut-offs assessed at 1%, 2%, 3% and 5% for both normally and reversely discordant data. This subset of the data was subsequently screened for outliers using the $^{206}Pb/^{238}U$ age of individual analyses. Both a weighted mean $^{206}Pb/^{238}U$ age and concordia age were determined for all discordance intervals, where possible. All ages discussed in the text are concordia ages unless otherwise noted, and analytical uncertainties are reported at 2σ. The discordance limit used for a given sample age is reported alongside the data in Table 5, along with the number of analyses ($n$) and number of unique zircon grains ($n_z$) used in the age calculation. Ages and age uncertainties are reported as calculated using the IsoPlot 3.75 for Excel package (Ludwig, 2003).

### 5.a. Three Bays Pluton

Zircon U–Pb ages were determined for three samples of fayalite granite, one sample of fayalite monzonite and one sample of ferrodiorite (ferromonzogabbro). Zircon in Three Bays Pluton granitoid samples are < 1 mm in diameter and form stubby prismatic, ovoid and blocky crystals (Fig. 8a). Backscatter images reveal either homogeneous internal structure or weak oscillatory zonation, and lack features indicative of subsequent alteration or recrystallization.

Ages obtained for Three Bays Pluton lithologies agree well with the *c.* 1290 Ma emplacement age originally proposed by Miller *et al.* (1997) for the Notakwanon Batholith. A single-sample date of

https://doi.org/10.1017/S0016756821000388 Published online by Cambridge University Press

**Table 5.** Summary of U–Pb zircon ages for rocks in the Flowers River area.

| Sample | Lithology | Concordia age (inherited age) (Ma) ±2$\sigma$ | MSWD (inherited age) | $n$ | $n_z$ | Weighted mean $^{206}Pb/^{238}U$ age (Ma) ±2$\sigma$ | MSWD | Discordance cut-off (%) |
|---|---|---|---|---|---|---|---|---|
| Three Bays Pluton | | | | | | | | |
| T0001 | Fayalite granite | 1293 ± 3 | 2.2 | 15 | 5 | 1291 ± 6 | 1.8 | 1 |
| T0015 | Fayalite granite | 1289 ± 2 | 1.9 | 30 | 6 | 1290 ± 2 | 0.69 | 1 |
| T0043 | Fayalite granite | 1289 ± 4 | 1.6 | 10 | 6 | 1291 ± 5 | 0.63 | 2 |
| T0045 | Fayalite monzonite | 1292 ± 4 | 1.7 | 13 | 5 | 1290 ± 5 | 0.95 | 3 |
| T0127 | Ferromonzogabbro | 1300 ± 14[a] | 1.19 | 8 | 4 | 1299 ± 9 | 3.5 | – |
| T0132 | Subsolvus granite | 1294 ± 7 (2557 ± 23) | 0.83 (0.38) | 9 (5) | 6 (5) | 1291± 8 (2553 ± 48) | 1.02 (3.2) | 1 |
| Flowers River Granite | | | | | | | | |
| T0004 | Peralkaline granite | 1281 ± 6 | 0.37 | 10 | 4 | 1283 ± 9 | 5.2 | 2 |
| T0008 | Peralkaline granite | 1280 ± 4 | 0.7 | 8 | 8 | 1275 ± 11 | 8.4 | 1 |
| T0030 | Peralkaline granite | 1281 ± 5 | 0.82 | 11 | 9 | 1281 ± 8 | 1.9 | 3 |
| T0124 | Hornblende granite | 1281 ± 5 | 2.9 | 13 | 3 | 1279 ± 5 | 0.49 | 1 |
| T0126 | Peralkaline granite | 1282 ± 3 | 2.9 | 28 | 17 | 1280 ± 4 | 1.4 | 1 |
| T0136 | Peralkaline granite | 1279 ± 3 | 1.7 | 15 | 9 | 1278 ± 5 | 1.7 | 2 |
| Nuiklavik Volcanics | | | | | | | | |
| T0009A | Lithic tuff | 1293 ± 12 | 0.64 | 6 | 6 | 1288 ± 5[b] | 0.78[b] | 3 |
| T0009B | Lithic tuff | 1290 ± 5 | 2.2 | 9 | 9 | 1288 ± 5[b] | 0.78[b] | 1 |
| T0021 | Crystal tuff | 1276 ± 6 | 0.74 | 10 | 6 | 1276 ± 6 | 1.18 | 2 |
| T0026A | Quartz porphyry | 1271 ± 3 | 0.74 | 20 | 14 | 1271 ± 4 | 1.6 | 1 |
| T0049 | Crystal tuff | 1271 ± 6 | 1.8 | 12 | 5 | 1269 ± 7 | 1.03 | 1 |
| T0085 | Alkali feldspar porphyry | 1281 ± 7 | 0.85 | 13 | 8 | 1278 ± 8 | 0.33 | 3 |
| T0091 | Alkali feldspar porphyry | 1282 ± 4 | 1 | 8 | 7 | 1281 ± 5 | 0.7 | 1 |
| T0101 | Quartz porphyry | 1275 ± 8 | 2.2 | 8 | 4 | 1272 ± 9 | 0.52 | 1 |

[a]Upper intercept age.
[b]Value from pooled result using data from both T0009A and T0009B.

1289 ± 2 Ma for a fayalite granite is the most precise age obtained for this group (sample CXAT0015; Fig. 9). A small number of *c.* 1330 Ma zircon ages are present among the < 3% discordant $^{206}Pb/^{238}U$ age populations; these may represent inheritance from older pulses of magmatism. A comparable upper intercept age of 1300 ± 14 Ma is obtained for the ferromonzogabbro.

### 5.b. Flowers River Granite

Zircon in Flowers River Granite shows considerable morphological diversity. Samples obtained from the margins of the central pluton are dominated by pristine euhedral zircon 1–3 mm in diameter (Fig. 8b) that locally comprises up to 2.5% of the modal mineralogy. These have a stubby prismatic habit and preserve well-defined, oscillatory magmatic zoning. The $^{206}Pb/^{238}U$ ages for these grains are broadly uniform around *c.* 1281 Ma, but a sparse population of *c.* 1330 Ma zircon analyses are also present. The most precise single-sample concordia ages obtained are 1282 ± 3 Ma and 1279 ± 3 Ma (Fig. 9).

Zircon morphologies in samples obtained proximal to the caldera reflect greater degrees of post-crystallization disturbance. A prevalent feature of this zircon is its amoeboid geometry (Fig. 8c), which is observed to truncate or overgrow an original magmatic zonation in BSE images. Interspersed among these are small, fractured, euhedral rhomb- and block-shaped zircons, whose internal structures are convolute and patchy. In most samples, zircon shows elevated levels of common Pb contamination, which is addressed using a $^{204}Pb$-based correction. Much of the $^{204}Pb$-corrected $^{206}Pb/^{238}U$ age distribution within this population overlaps with the *c.* 1281 Ma date obtained from the less-disturbed samples. A diffuse assortment of younger ages is also present within the data, spanning 540 to 1220 Ma, interpreted to reflect either ancient Pb loss or mixing between two or more discrete age domains.

### 5.c. Nuiklavik Volcanics

Zircon phenocrysts are abundant in most crystal-rich facies within the caldera, but are almost entirely absent from aphyric ash-flows and ignimbrites. Internal structure is rarely evident in backscatter images and, where present, appears as faint oscillatory zonation. Crystal size and morphology once again ranges from prismatic

https://doi.org/10.1017/S0016756821000388 Published online by Cambridge University Press

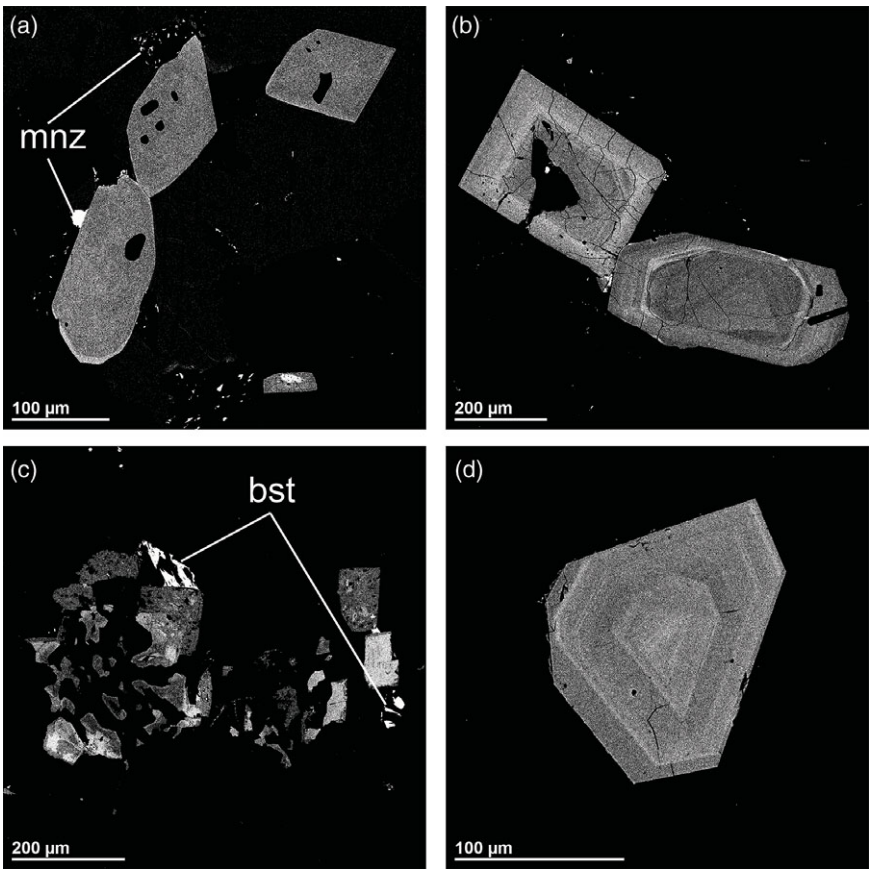


**Fig. 8.** (Colour online) Contrast-enhanced SEM-BSE images of zircon specimens in the Flowers River area. (a) Zircon from a Three Bays augite-fayalite granite (CXAT0001) showing homogeneous internal structure. (b) Euhedral zircons from an equigranular Flowers River Granite (Sample CXAT0126) with prominent oscillatory zonation. (c) Zircon from a porphyritic Flowers River Granite (Sample CXAT0030) with irregular amoeboid geometry. Relict, concentric internal structures are weakly preserved in some parts of the crystals and may indicate partial dissolution of a primary zircon crystal. These may alternately be pseudomorphs of an earlier Zr-bearing phase. (d) Zircon from a Nuiklavik porphyry (CXAT0046) showing concentric magmatic zonation. Mineral abbreviations: bst – bastnäsite-(Ce), mnz – monazite-(Ce). Inclusions in (a) and (b) are of apatite and alkali feldspar.

to blocky (Fig. 8d), as in intrusive lithologies, but subhedral crystal fragments thereof are also prevalent.

Age data for Nuiklavik volcanic rocks define three distinct groups (Fig. 10): the oldest yields a concordia age of 1290 ± 5 Ma; the intermediate population a concordia age of 1282 ± 4 Ma; and the youngest a concordia age of 1271 ± 6 Ma. Although the older two populations overlap within error, these sample sets may also be distinguished on petrologic and geochemical criteria (see Section 6.b).

### 5.d. Subsolvus granite

Two concordia ages are obtained from a single sample of subsolvus granite (Sample CXAT0132), and weakly discordant analyses from the older population define a discordia line between them (Fig. 11). The older of these concordia ages is 2557 ± 23 Ma, and the younger is 1293 ± 8 Ma.

## 6. Discussion

### 6.a. Age of the Flowers River suite

The Flowers River Granite records an emplacement age of *c.* 1281 Ma. This result is within error of the original 1271 ± 15 Ma age presented by Hill (1991). Similarly, Collerson (1982) reported a comparatively young whole-rock Rb–Sr errorchron age of 1262 ± 7 Ma for peralkaline granite to the NE of the study area; however, revisions have since been proposed for the $^{87}$Rb decay constant used by Collerson (1982). When adjusted for a $^{87}$Rb decay constant of (1.3972 ± 0.0045) × 10$^{-11}$ a$^{-1}$ (Villa *et al.* 2015), the data yield an age of 1281 ± 3 Ma (MSWD = 1.2), which is in good accord with the U–Pb ages reported here for the Flowers River Granite. Alternatively, when adjusted for a decay constant of 1.408 × 10$^{-11}$ a$^{-1}$ (Gargi, 2019), the data provide an age of 1271 ± 3 Ma (MSWD = 1.2), which overlaps with U–Pb ages obtained here for a subset of the Nuiklavik Volcanics (Section 6.3). No peralkaline granite samples analysed in this study provided an age in this range and, on this basis, the result using the decay constant of Villa *et al.* (2015) is favoured. Nevertheless, the existence of a peralkaline intrusive phase coeval with the youngest volcanic lithologies cannot be ruled out (see Section 6.3), and therefore either of these ages may be correct. Caution must also be exerted in assigning significance to Rb/Sr ages for peralkaline complexes, particularly given the locally pronounced subsolidus alteration observed in the Flowers River Granite (e.g. Borst *et al.* 2019). In any case, the age agreement tentatively indicates that the $(^{87}Sr/^{86}Sr)_i$ values obtained from these data may be reliable estimates of the whole-rock isotopic signature of the Flowers River Granite. Model I Rb–Sr calculations performed in IsoPlot 3.75 (Ludwig, 2003) provide a $(^{87}Sr/^{86}Sr)_i$ of 0.70808 ± 0.00015, compared with an originally reported value of 0.7080 ± 0.0018 (Collerson, 1982).

The Three Bays granitoids provide an age of *c.* 1290 Ma, coincident with the previously inferred age for the Notakwanon Batholith. Assuming the two are roughly coeval, the prior interpretation of the Notakwanon Batholith (and by extension, the Three

https://doi.org/10.1017/S0016756821000388 Published online by Cambridge University Press

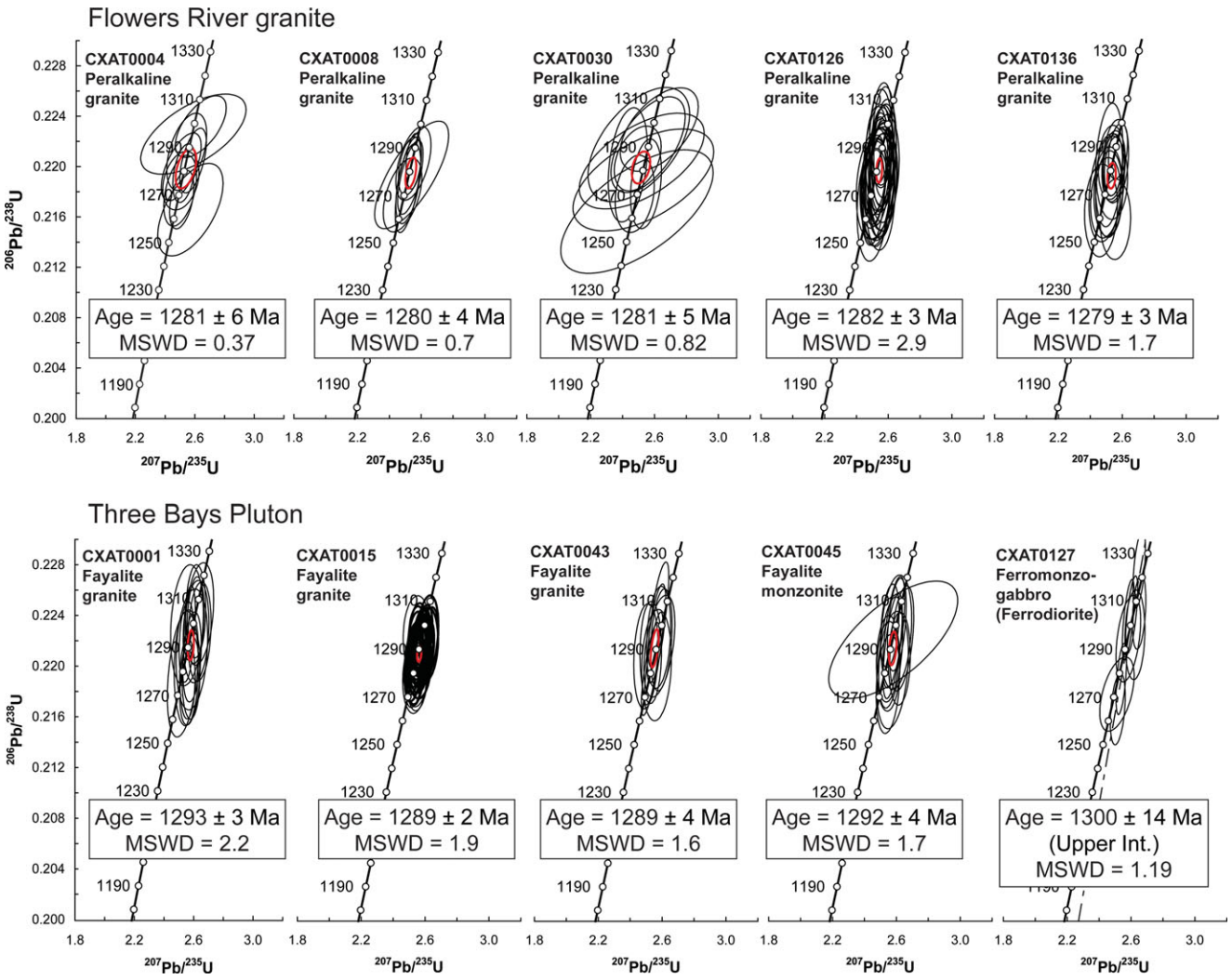


**Fig. 9.** (Colour online) Zircon U–Pb concordia diagrams for samples of Flowers River peralkaline granite (top row) and of the various Three Bays Pluton lithologies (bottom row). All reported ages are concordia ages, except for one upper intercept age reported for a ferromonzogabbro.

Bays Pluton) as the youngest of the typical AMCG-affinity intrusions in the Nain Plutonic Suite (Myers *et al.* 2008) is correct, and this style of magmatism can be concluded to have ceased regionally following the emplacement of these two plutons. A lag of several million years separates the Flowers River Granite from this latest episode of AMCG magmatism. While not unusual in a broader regional context – Myers *et al.* (2008) proposed five episodes of growth within the Nain Batholith – the abrupt shift to peralkaline compositions following this particular gap warrants additional scrutiny.

### 6.b. Archean crustal signature in the subsolvus granite

The subsolvus granite displays a geochemical signature sufficiently distinct to distinguish it from the other granitoid lithologies of the region. The younger concordia age obtained for the sample lies outside the error of the Flowers River suite. Although the age lacks the precision necessary to discount an origin unique from any of the suites discussed at length here, it most likely coincides with the emplacement of the Three Bays Pluton. Despite this, the rocks differ substantially from the Three Bays granitoids. The prevalence of gneissic xenoliths in outcrop, evident xenocrystic age inheritance, and their metaluminous to weakly peraluminous geochemistry strongly suggest that these are crustal melts produced in response to the thermal flux associated with TBP magmatism. If these are equivalent to the subsolvus granite reported by Collerson (1982) to the NE of the caldera, then the elevated $(^{87}Sr/^{86}Sr)_i$ reported for these rocks would support an origin via crustal anatexis, with or without variable degrees of mixing with the TBP granitoid magmas.

The inherited Neoarchean age present in these rocks indicates that the crust underlying the Three Bays and Flowers River plutons was involved in the amalgamation of the Hopedale and Saglek blocks. This may help to further constrain the geometry of the Hopedale–Saglek suture zone (e.g. Wasteneys *et al.* 1996; Hinchey & Corrigan, 2019). The coincidence of the FRIS astride a major Archean crustal suture introduces yet another lithosphere-scale structure, in addition to the Torngat Orogen and Gardar–Voisey's Bay Fault Zone (Fig. 1), that may have permitted the magmas within the Nain Batholith to attain their shallow emplacement depths (e.g. Hill, 1991; Myers *et al.* 2008). The previously overlooked importance of synmagmatic deformation and major structural corridors to the ascent and emplacement of massif anorthosite has recently led to the suggestion that AMCG

https://doi.org/10.1017/S0016756821000388 Published online by Cambridge University Press

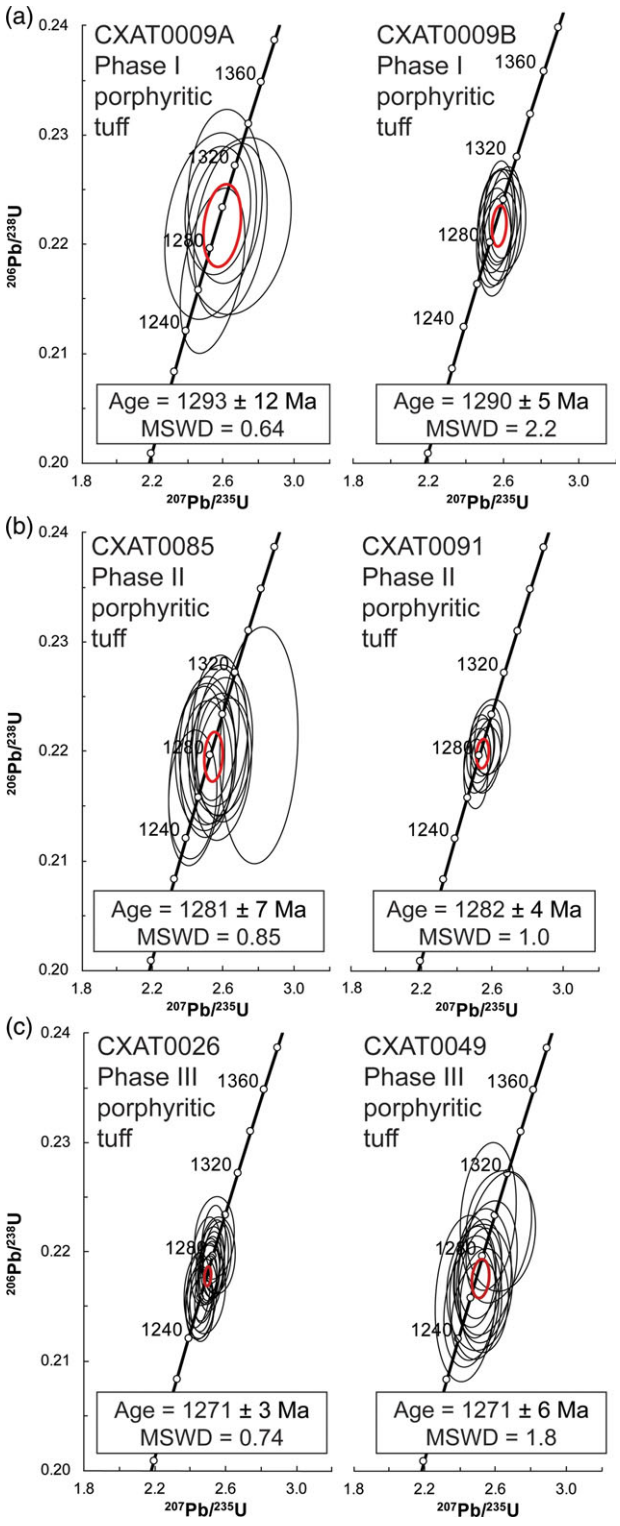


**Fig. 10.** (Colour online) Zircon U–Pb concordia diagrams with concordia ages for (a) old (Phase I), (b) intermediate (Phase II) and (c) young (Phase III) sample populations identified within the Nuiklavik Volcanics.

magmatism may be the product of more conventional tectonic regimes such as continental arcs (Slagstad *et al.* 2018; Lehmann *et al.* 2020). Although an arc setting is incompatible with the geodynamic framework of Labrador preceding the onset of Mesoproterozoic magmatism, structural conduits played a crucial role in the formation of the Nain Plutonic Suite.

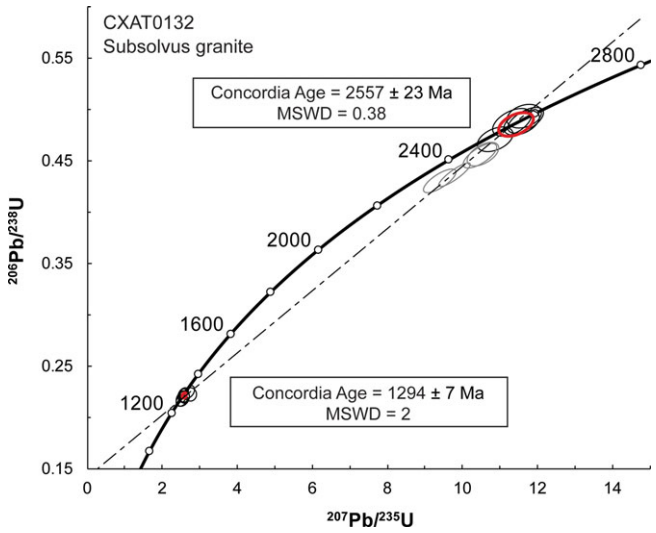


**Fig. 11.** (Colour online) Concordia plot showing U–Pb zircon ages for two concordant populations in sample T0132, a subsolvus granite from the Three Bays Pluton. The superimposed discordia line intersects both concordia ages and is defined by weakly discordant analyses within the older population.

### 6.c. Revised Nuiklavik caldera architecture

The Nuiklavik Volcanics have previously been treated as a single coherent volcanic assemblage, comagmatic with the Flowers River Granite (Hill, 1982; Miller, 1993). Instead, geochronological and geochemical data presented here support episodic volcanism that was linked to at least two distinct magmatic sources. The lowermost unit of the caldera is most easily discriminable, given that members of this unit are the only Nuiklavik rocks observed to contain plagioclase (albeit only in apparent lithic fragments). Relative to the other volcanic units, these rocks are comparatively undepleted in Ba and Sr, are not as enriched in incompatible elements and have 10 000×Ga/Al < 5. Zircon geochronology suggests these rocks were erupted at 1290 ± 5 Ma, coeval with emplacement of the Three Bays Pluton (Fig. 10). Combined with their similar Eu/Eu* (0.49–0.54) and FeO/(FeO+MgO) (0.87–0.90) values, these rocks are proposed to be comagmatic with a subset of the TBP granitoids. The previously reported ages of 1291 ± 2 and 1289 ± 1 Ma for the Nuiklavik Volcanics (Miller, 1994) were likely obtained from this unit.

Georeferenced geochemical data reported by Miller & Kerr (2007) for a large sampling of volcanic lithologies show that Nuiklavik rocks with Ba > 500 ppm were sampled overwhelmingly along the southwestern edge of the caldera. This coincides with the sampling location for the older rocks reported here. Accordingly, the mapping distribution of these Ba-rich samples is interpreted to represent exposures of this oldest subunit (Phase I). These rocks bear geochemical similarities to both the fayalite-bearing granitoids as well as to the subsolvus granite. It is not immediately apparent which of these magmas was parental to this episode of volcanism, or whether they are the products of some degree of magma mixing.

Two crystal-rich volcanic samples provide ages of 1281 ± 7 Ma and 1282 ± 4 Ma (Fig. 10), in good agreement with crystallization ages obtained for the Flowers River Granite (Phase II). Hematitic alteration (Fig. 7c) is characteristic of these samples, and they are the only volcanic lithofacies containing crystal fragments with granophyric texture. A third and final group (Phase III) yield concordia ages at 1271 ± 6 Ma and 1271 ± 3 Ma. These ages do not

https://doi.org/10.1017/S0016756821000388 Published online by Cambridge University Press

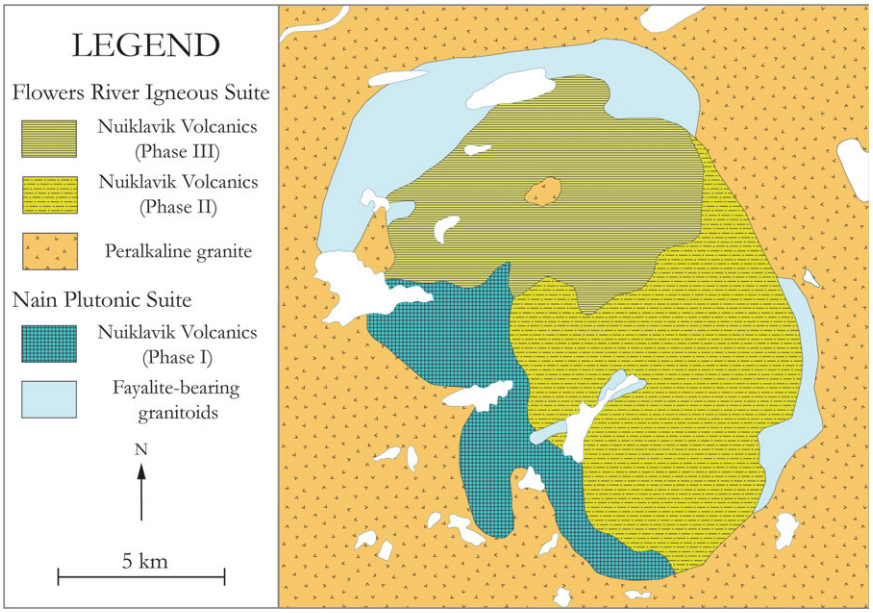


**Fig. 12.** (Colour online) Geological map of the Nuiklavik caldera showing estimated extents of preservation for each of the inferred phases of volcanism. All mapped contacts between separate volcanostratigraphic units are interpolated from georeferenced geochemical data, with contacts inferred from topography. Modified after Miller (1993).

coincide with that of any intrusive phase encountered in the study area, but overlap with emplacement ages reported for the Harp Dykes, which intrude peripherally around the Three Bays Pluton and Flowers River Igneous Suite (Cadman *et al.* 1993). However, Phase III sample geochemistry is broadly indistinguishable from that of Phase II volcanism. These samples are sufficiently young relative to the Flowers River Granite to discount a single, sustained magmatic episode. Accordingly, this youngest phase of volcanism is interpreted to reflect renewed anatexis of a source parental to the Flowers River Granite resulting from sustained regional uplift (e.g. Hill, 1991), regional heating associated with emplacement of the Harp Dykes, or both.

A revised caldera map (Fig. 12) reflecting the new, three-phase interpretation of volcanism has been constructed by combining the detailed volcanostratigraphic mapping of Miller (1993) with first-hand field observations, U–Pb data and georeferenced geochemical data from Miller & Kerr (2007). Our field observations do not indicate any strict correlation between volcanostratigraphic position and the proportional abundance of porphyritic and aphyric volcanofacies. Porphyritic and aphyric samples were obtained from each of the three subunits proposed here. Mapping of these subunits is informed primarily by U–Pb results and geochemistry and, as such, is not fully compatible with the interpretations of Miller (1993). However, it is likely that similar lithofacies successions would arise in the geochemically similar Phase II and Phase III events, and that these would not be trivial to differentiate from a purely volcanological standpoint. Accordingly, it is suggested that the two interpretations be used in concert for future investigations.

### 6.d. Petrogenetic implications

The geochronology presented here supports the inclusion of the FRIS within the broader magmatic context of the Nain Batholith (Myers *et al.* 2008). Moreover, the Flowers River Granite was emplaced only several million years after the local expression of this long-lived regional AMCG magmatism. The Flowers River area is also the only locality within the Nain Batholith currently known to have experienced multiple episodes of magmatism around the same focal centre; elsewhere in the Nain Plutonic Suite, this is similarly true only to the west where other late peralkaline intrusions occur. Given this close spatial relationship and the similar age and geochemistry of the Flowers River Granite and TBP granitoids, it appears likely that certain aspects of the Flowers River Granite differentiation path were shared with or inherited from the older TBP magmas.

One sample of fayalite granite (CXAT0015) displays a weakly peralkaline chemistry (Agpaitic Index, AI = 1.01). This sample displays pronounced subsolidus alteration to its bulk mineralogy, including large inclusion-rich crystals of aegirine-augite not unlike those observed in the Flowers River Granite. The extensive alteration in this sample suggests that its peralkaline signature was produced by metasomatic addition of alkalis, and this may raise similar questions concerning the origin of the peralkaline signature of the Flowers River Granite itself. Whereas the aegirine-augite in the Flowers River Granite displays a similar morphology to that of the fayalite granite, the Flowers River Granite also contains magmatic specimens of aenigmatite and common peralkaline amphiboles optically identified to range from richterite to katophorite to arfvedsonite (Strong & Taylor, 1984) that do not occur in the fayalite granite. Inclusion-rich crystals of aegirine-augite are widely dispersed even among samples of peralkaline granite recording the lowest degrees of subsolidus alteration, suggesting that this aegirine-augite is perhaps a common product of reactions triggered *in situ* by evolution of a fluid phase. Such phenomena have become increasingly documented at other silicic peralkaline complexes (e.g. Vasyukova & Williams-Jones, 2014; Vilalva *et al.* 2016; Yang *et al.* 2020). Meanwhile, the weakly peralkaline fayalite granite is exposed within the central Flowers River Granite pluton, meaning that its present mineralogy may have been produced by interaction with these same fluids.

Plagioclase is perhaps the most important fractionating or refractory (e.g. Emslie *et al.* 1994) mineral for producing the geochemical signatures observed in AMCG-affinity rocks. Plagioclase

https://doi.org/10.1017/S0016756821000388 Published online by Cambridge University Press

fractionation has similarly been explored as a driver of magma evolution towards peralkaline compositions, dubbed the 'plagioclase effect' in this context (Bowen, 1945; Frost & Frost, 2013). Attempts to validate this connection experimentally have yielded mixed results, despite its existence being supported by numerous natural occurrences (Kovalenko *et al.* 2006). Silicic peralkaline magmatism is now more commonly proposed to require a pre-enriched mantle source in addition to extensive fractionation and crustal contamination to produce the observed high degrees of incompatible element enrichment (e.g. Larsen & Sørensen, 1987; Kramm & Kogarko, 1994; Markl *et al.* 2010). The parental transitional to alkalic basaltic melts so produced fractionate through metaluminous trachytic compositions before ultimately attaining peralkalinity (Romano *et al.* 2018; Chen *et al.* 2019). By contrast, most AMCG-affinity magmas have been proposed to feasibly derive from high-pressure or polybaric fractionation of a tholeiitic, rather than transitional or alkalic, basaltic melt (e.g. Charlier *et al.* 2010; Frost & Frost, 2013). There are few crustal alternatives for peralkaline melt generation, and these generally simply require that mantle-sourced fluids penetrate to more shallow depths (Martin, 2006). However, a crustal origin for the granitoids of AMCG complexes is more widely supported than the mantle-derived alternative (e.g. Emslie *et al.* 1994; McLelland *et al.* 2010; Ashwal & Bybee, 2017). The close spatiotemporal association and geochemical similarity between the TBP granitoids and Flowers River Granite suggests that one of the two suites marks a departure from the source typically attributed to its respective petrogenetic family.

The common inference that AMCG-affinity granitoids are the products of crustal melting is based in part on their isotopic and trace-element compositions, field relationships among the various associations within an AMCG complex, as well as a perceived paucity of compositionally intermediate material (Emslie *et al.* 1994; McLelland *et al.* 2004). Petrogenetic features argued elsewhere to necessitate a mantle source for AMCG granitoid magmas are their low $fO_2$ and high FeO/(FeO+MgO), features most easily reconciled with direct fractionation of a mantle-derived tholeiite as noted above, or by delayed partial melting of a crystallized differentiate thereof (e.g. Frost & Frost, 1997, 2008*a*). Creaser *et al.* (1991) showed that only when given a source of tonalitic to granodioritic composition (with added stipulation by Frost & Frost (1997) that it must also be ilmenite-bearing) can anhydrous, low-$fO_2$ and highly ferroan compositions be reproduced via crustal anatexis. Gneiss of tonalitic to granodioritic composition is notoriously abundant in Archean terranes, and it is not unreasonable to think that rocks of this composition could be voluminously represented in the underlying Hopedale Block. On these grounds, a crustal origin for the TBP granitoids cannot be fully discounted. However, the anorthosite and ferrodiorite exposed in the study area are unusually alkali-rich (Hill, 1988; this study), and the TBP granitoids display higher agpaitic indices (AI, or molar $(Na_2O + K_2O)/Al_2O_3$) and incompatible element concentrations than are typical of comparable rocks elsewhere in the Nain Batholith. Accounting further for the later episode of peralkaline magmatism, it is difficult to argue that the anorthosite, ferrodiorite, TBP granitoids and Flowers River Granite each acquired their enrichment independently while being the products of multiple distinct sources. It therefore appears likely that these magmas either all experienced substantial contamination by an unidentified but extensive incompatible-element-enriched lower crustal reservoir, or that they were all sourced directly from an enriched reservoir residing in the lower crust or lithospheric mantle. Given the lack of evidence to support the existence of such a contaminant, the limited set of conditions under which crustal melting can produce ferroan liquids and the prohibitively silica-poor compositions of some of the ferrodioritic rocks (e.g. Morse, 1991), the most probable scenario is that all of the associations in the study area share a common source located in the lithospheric mantle.

Following a liquid evolution line consisting of ferrodiorite, fayalite monzonite, fayalite granite and peralkaline granite, each successive unit displays stronger negative Eu anomalies, FeO/(FeO+MgO) approaching unity, progressive depletion of Ba, Ti, Sr and P, and enrichment in REE, Y, Zr and Nb (Fig. 6). Many of these trends are consistent with sustained fractionation of plagioclase and/or alkali feldspar, along with apatite, Fe–Ti oxides and ferromagnesian silicates. Alkali feldspar (with or without plagioclase) is present among all of the lithologies in question, whereas apatite is an abundant phase (2–5%) only in ferrodiorite and fayalite monzonite. These observations broadly align with geochemical features expected to accompany extensive fractionation along a tholeiitic trend. Furthermore, under a polybaric crystallization regime (e.g. Charlier *et al.* 2010; Bybee *et al.* 2014), a ferrodiorite of similar composition to those exposed in the study area would be capable of generating late peralkaline liquids. Accordingly, a genetic link between the TBP ferrodiorites, TBP granitoids and the Flowers River Granite appears difficult to dispute. However, a direct relationship via crystal fractionation is not supported by the geochronology presented here for the complex, since it is unlikely that a continuously evolving melt could have persisted in the middle crust for a *c.* 8 Ma interval without having produced material of intermediate age. Instead, the Flowers River Granite is more consistent with fractionation of a discrete anatectic melt generated from residual ferrodioritic cumulates preserved in the lower or middle crust, a scenario proposed previously for AMCG-affinity granitoids by Frost & Frost (1997). Whether this can be similarly extended to the older fayalite granite is not resolvable in the ages obtained here. If this were the case, it could explain the relative low abundances of intermediate compositions throughout the Nain Batholith as noted by Emslie *et al.* (1994). Another possibility is that the Flowers River Granite differentiated directly from a penecontemporaneous generation of mantle melt; however, such a liquid would require its own cycle of plagioclase fractionation (and perhaps resultant anorthosite genesis) in order to replicate the geochemical features observed in the TBP granitoids. At present, there is no evidence to support two discrete anorthosite genesis events in the study area. In light of this, we favour an anatectic origin for the FRIS; however, geochronological identification of a bimodal age distribution within the surrounding anorthosite could render the alternative scenario more plausible.

### 6.e. Lithotectonic sources for localized enrichment

Localized enrichment of the sub-continental lithospheric mantle underlying southern tip of the Nain Batholith is consistent with the spatial distribution of major lithotectonic boundaries near the Flowers River area. The entire length of the lithosphere intruded by the Nain Batholith was directly affected by the Torngat Orogeny (1920–1800 Ma), with the consequent terrane suture playing a major role in controlling magmatic ascent and emplacement along the boundary separating the Southeastern Churchill Province and North Atlantic Craton (Myers *et al.* 2008). Only the southernmost extents of this region would have thereafter experienced peripheral effects of the Labradorian Orogeny (1710–1600 Ma; Gower *et al.* 1997), the Makkovikian–

https://doi.org/10.1017/S0016756821000388 Published online by Cambridge University Press

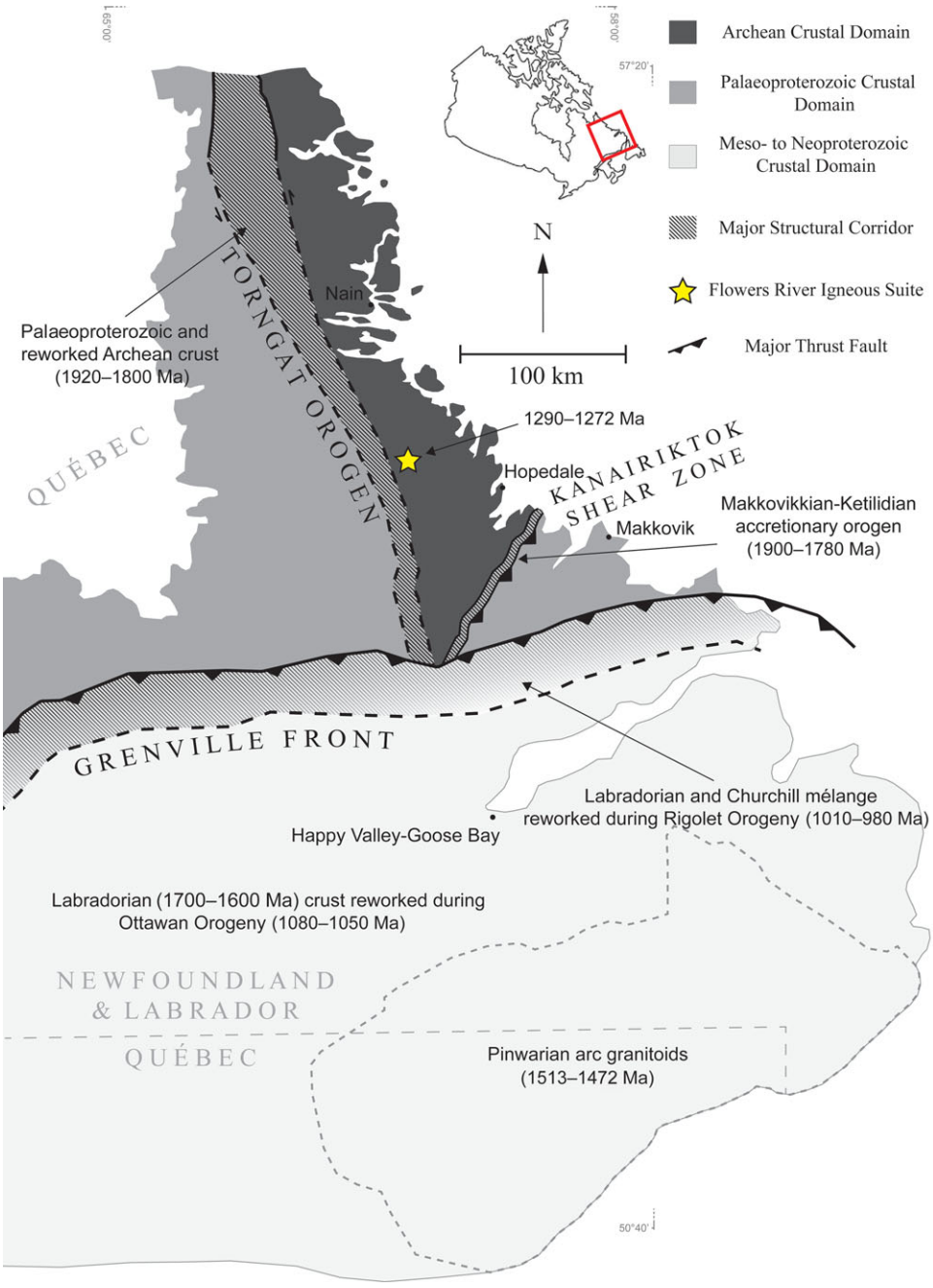


**Fig. 13.** (Colour online) Map detailing the major lithotectonic elements present in Labrador and eastern Québec. The site of Flowers River magmatism is close to three major lithotectonic boundaries: the Torngat Orogen (*c.* 1920–1800 Ma; Myers *et al.* 2008), the Makkovikian(-Ketilidian) arc-accretion boundary (*c.* 1850–1720 Ma; Gandhi *et al.* 1969) and the Grenville Front (*c.* 1080–980 Ma; Rivers & Corrigan, 2000). The Grenville Front represents reworked allochthonous or parautochthonous material of the Labradorian Orogeny (*c.* 1700–1600 Ma; Gower & Krogh, 2002), and arc granitoids of the Pinware Terrane (*c.* 1513–1472 Ma; Rivers & Corrigan, 2000) are located south of the Grenville Front. The Torngat Orogen was a doubly vergent, E–W transpressional event, while the Makkovikian, Labradorian and Pinwarian events involved either primarily N-vergent or doubly vergent N–S subduction or arc accretion events. Although these events are at variable distances from the southern Nain Batholith, they are of suitable orientation and magnitude to have enriched the lithosphere prior to melt extraction at *c.* 1364 Ma. The localization of much of the nearby Palaeoproterozoic to earliest Mesoproterozoic tectonic activity towards the south may have exposed the southernmost portions of the lithosphere to a greater degree of enrichment, ultimately producing the highly enriched magmas that gave rise to the Three Bays Pluton and Flowers River suites.

Ketilidian Orogeny (1900–1780 Ma; Gandhi *et al.* 1969) and the more distal Pinwarian Orogeny (1530–1450 Ma; Rivers & Corrigan, 2000; Fig. 13). This confluence of suprasubduction zone corridors may have localized enrichment within the orogen-proximal lithosphere underlying the southern limits of the Nain Batholith. A comparable model was put forth by Siegel *et al.* (2017) for the Strange Lake intrusion, who noted its possible wider applicability to peralkaline occurrences throughout the Nain Plutonic Suite. Moreno *et al.* (2016) proposes a similar origin for peralkaline granites in Egypt, citing slab-derived carbonatitic

https://doi.org/10.1017/S0016756821000388 Published online by Cambridge University Press

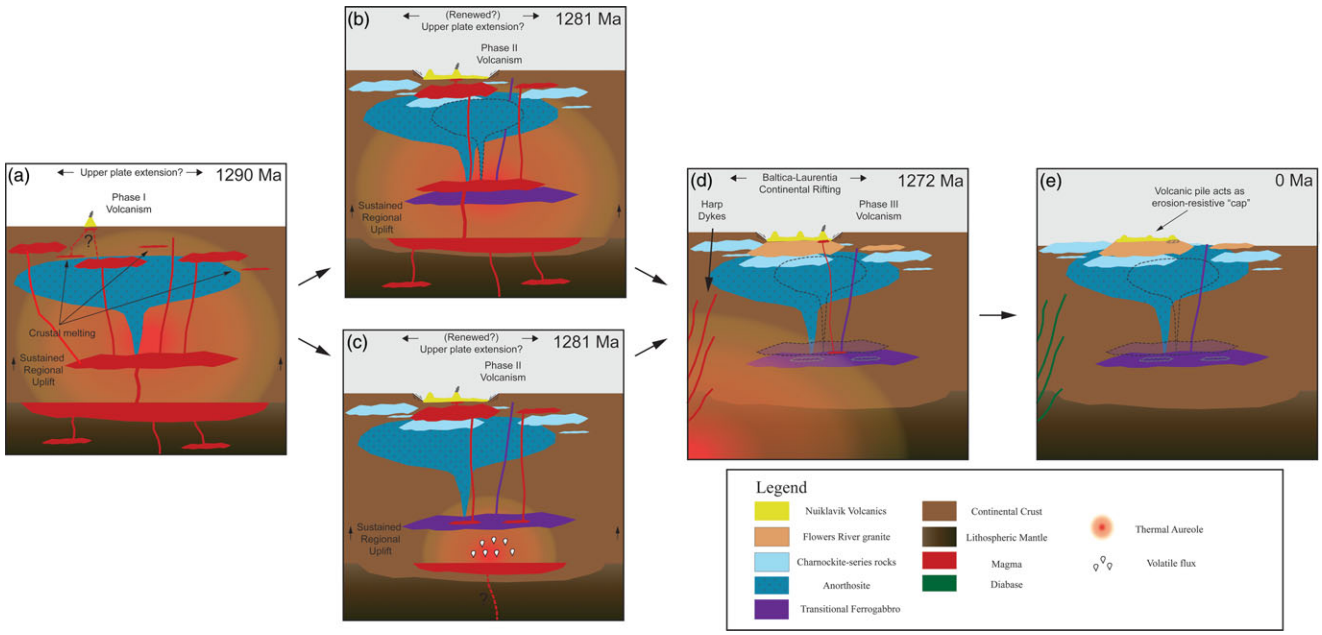


**Fig. 14.** (Colour online) Simplified model outlining the evolution of the Flowers River area. (a) Anorthosite and mangerite-charnockite series rocks are derived from a transitional to alkalic basaltic liquid ponded in the lower crust. Heat associated with the intrusions simultaneously produces crustal partial melts. The Phase I Nuiklavik Volcanics are emplaced, deriving from one of the two melt sources or from mixing between them. (b) One of two possible origins for the Flowers River Igneous Suite. A second pulse of anorthositic diapirism occurs, while the granitoid rocks generated in this instance achieve silicic peralkaline compositions via fractionation and crustal assimilation. The eruptible fraction of these magmas (the Phase II volcanics) induces caldera collapse in the overlying volcanic centre. (c) Alternative model where mantle-sourced volatiles induce partial melting of the crystallized ferrogabbroic residue in the lower crust. As in (b), eruption of the Phase II volcanics induces caldera collapse. (d) Craton-scale tholeiitic magmatism produces the Harp Dyke swarm, the peripheral thermal effects of which induce a second partial melting event and emplacement of the Phase III volcanics. A second caldera collapse event is possible. (e) Erosion creates the modern exposures of the complex. The erosion resistance of the silicic volcanic pile acts as a 'cap' for the underlying granite pluton, resulting in the caldera's high modern topographic relief.

metasomatism of the lithospheric mantle (e.g. Poli, 2015; Chen *et al.* 2018) that persisted following the Pan-African Orogeny. This rationale may also be applicable to the Gardar Province, which lies between two Palaeoproterozoic orogens in Greenland's Ketilidian and Nagssugtoqidian belts (van Gool *et al.* 2002; Upton, 2013). Comparatively, however, the Gardar Province experienced flare-ups in magmatic activity over an extended period (1350–1140 Ma), and products of this magmatism spanned a far greater compositional range than has been documented in any single peralkaline occurrence in Labrador (Upton *et al.* 2003).

In the model proposed here, the TBP follows a typical AMCG style of emplacement (Fig. 14a; Ashwal, 1993; Emslie *et al.* 1994). Thereafter, the transition to peralkaline magmatism at *c.* 1281 Ma resulted either from renewed melting of the enriched lithospheric mantle (Fig. 14b), or from anatexis of a residual ferrodioritic reservoir in the lower crust and/or its intermediate differentiates (Fig. 14c). A third and final episode of magmatism, recorded by the Phase III Nuiklavik Volcanics at *c.* 1272 Ma, resulted from further uplift and thermal perturbation associated with the emplacement of the Harp Dykes, which represent a local subset of broadly asthenosphere-derived melts that were associated with the Mesoproterozoic break-up of the supercontinent Nuna and were emplaced throughout Laurentia and Baltica (Cadman *et al.* 1994; Bartels *et al.* 2015; Fig. 14d). The erosion-resistant volcanic cap preserved the caldera and the underlying plutonic rocks, and is responsible for its elevated modern relief (Fig. 14e).

The tectonic emplacement mechanism underlying the Nain Plutonic Suite, and by extension the TBP and FRIS, remains poorly constrained. Proposed drivers of magmatism have included upper plate extension in a far-field continental back-arc setting (e.g. Rivers & Corrigan, 2000), a mantle superswell underlying Laurentia (Hoffman, 1989; Hill, 1991) or migration of a subducted spreading centre (Gower & Krogh, 2002; McLelland *et al.* 2010). The latter functions best for the older plutons in the Churchill Province that young northwards (Gower & Krogh, 2002), but no similar spatial pattern is evident in pluton ages for the Nain Batholith. The local juxtaposition of supracrustal rocks with mid-crustal AMCG rocks has led to the conclusion that magmatism in the Flowers River area coincided with a persistent interval of seemingly permanent regional uplift (Hill, 1991); on this basis, Hill favoured the superswell model, but ultimately argued for a lower crustal quartzofeldspathic source for the Flowers River Granite.

The protracted geodynamic activity ongoing in Laurentia throughout the Proterozoic Eon is elsewhere implicated in the genesis of numerous magmatic complexes of variable affinity, including continental arcs (e.g. Hanmer *et al.* 2000), island arcs (e.g. Sappin *et al.* 2011), and continental rift-related mafic intrusions and lavas (Cadman *et al.* 1994; Hinze *et al.* 1997), in addition to many post-orogenic AMCG complexes (e.g. Emslie & Hegner, 1993; Corrigan & Van Breemen, 1997). Rivers & Corrigan (2000) and Hynes & Rivers (2010) both advocate for a long-lived, Andean-type margin along southern Laurentia (modern coordinates) that remained active throughout much of the Proterozoic Eon. Pauses or polarity reversals at this distal subduction zone, and the reciprocal cessation of local upper plate extension, could explain the intermittent gaps in the Nain Plutonic Suite age record (Myers *et al.* 2008). This model of upper plate extension appears most consistent with the current petrochronological

https://doi.org/10.1017/S0016756821000388 Published online by Cambridge University Press

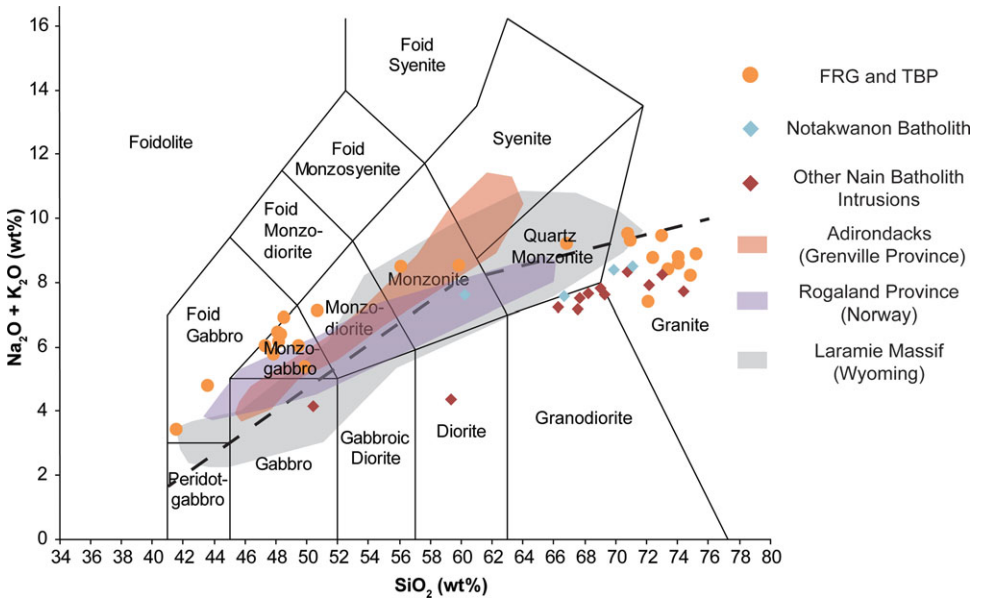


**Fig. 15.** (Colour online) Total alkalis versus silica plot for ferrodioritic and granitoid lithologies from a selection of AMCG complexes worldwide. The Flowers River Granite (FRG) and Three Bays Pluton (TBP) define a gently arcuate, moderately alkalic trend from foid gabbro to granite. Whole-rock analyses of other Nain Batholith intrusions (Umiakovik Batholith and Makhavinekh Pluton; see Fig. 1) have lower total alkali contents and may define a trend along the upper boundary from gabbro to granite, although a paucity of data from intermediate compositions leaves this to inference. The Notakwanon Batholith plots just above the more northerly Nain Batholith intrusions, although one intermediate sample shows moderate enrichment in alkalis. Compositional ranges are superimposed for geochemical data published for the Adirondack Massif (USA), Rogaland Anorthosite Province (Norway) and Laramie Anorthosite Massif (USA). Plot boundaries after Middlemost (1994). Data sources: Flowers River area: Collerson (1982), Hill (1988) and this study; Notakwanon Batholith: Emslie & Stirling (1993); Nain Batholith: Ryan (1991), Emslie & Loveridge (1992) and Emslie & Stirling (1993); Adirondack Massif: Seifert *et al.* (2010); Rogaland Province: Vander Auwera *et al.* (1998); Laramie Massif: Mitchell *et al.* (1996), Scoates *et al.* (1996), Frost *et al.* (1999) and Anderson *et al.* (2003).

framework of the Nain Batholith. A subsequent transition to more typical tholeiitic, asthenosphere-sourced magmatism in the form of the Harp Dykes may have helped to sustain the seemingly 'permanent' regional uplift.

### 6.f. Comparison with other AMCG complexes

Whereas the lithological make-up of the Nain Plutonic Suite is largely in line with that of AMCG complexes worldwide, the unique emplacement setting of the Nain Plutonic Suite should be reflected in petrogenetic departures from a typical, post-collisional AMCG suite. A total alkalis versus silica plot shows that the TBP ferrodiorites are enriched relative to the ferrodiorites of other AMCG complexes, particularly those from other intrusions in the Nain Batholith (Fig. 15). The Rogaland (Norway), Laramie (central USA) and Adirondack (northeastern USA) massifs all show linearly increasing trends in alkali content relative to silica, although the overall slope of this differentiation trend varies at each locality. Comparatively, the Flowers River Granite and TBP granitoids with > 70 wt% $SiO_2$ have lower total alkalis, defining a gently curved trend. The Flowers River magmas were able to attain peralkaline compositions despite their lower absolute alkali content, indicating that alkali feldspar could not have been solely responsible for the removal of Al from the evolving magma. If the Flowers River magmas did arise by anatexis of a material related to, but more compositionally evolved than, ferrodiorite (i.e. the fayalite monzonite), significant volumes of restitic plagioclase could feasibly produce an initial liquid sufficiently depleted in Al that would fractionate towards moderately peralkaline compositions.

The intimate association between AMCG magmatism and long-lived convergent margins (McLelland *et al.* 2010; Ashwal & Bybee, 2017) precludes their isolation from the metasomatic enrichment processes proposed here to account for the FRIS. Furthermore, the modest comparative enrichment of the most primitive TBP lithologies relative to post-collisional equivalents (Fig. 15) suggests that pre-enrichment of the mafic precursor alone cannot account for the transition to peralkaline magmatism in the Flowers River area. Instead, the atypical tectonic environment that fostered the Nain Plutonic Suite appears to have played a key role in the late compositional shift. It is possible that low degrees of partial melting of the ferrodioritic to mangeritic rocks in many AMCG complexes would yield liquids that fractionate toward a peralkaline chemistry. However, production of such a second generation of magma may have been inhibited by the absence of a renewed thermal anomaly, or by preceding or subsequent crustal thickening in these localities that did not occur in Labrador.

## 7. Summary

The Flowers River Igneous Suite was emplaced at 1281 Ma, intruding 1290 Ma AMCG-affinity rocks in the vicinity of Sango Bay. These magmatic suites represent the youngest two episodes of plutonism associated with the Mesoproterozoic assembly of the Nain Batholith. Both of these events were accompanied by a period of coeval volcanism, with a third volcanic event at *c.* 1272 Ma having possibly been triggered by lithospheric extension and coeval emplacement of the Harp Dyke swarm (Cadman *et al.* 1994).

The Flowers River Igneous Suite is the product of protracted differentiation of a material of initially transitional to alkali basaltic composition, derived from a region of the lithospheric mantle that had previously been enriched by interaction with slab-derived volatiles. This liquid initially gave rise to moderately alkalic ferrodiorites and metaluminous mangerite-charnockite series rocks of the Three Bays Pluton, before the system ultimately attained peralkaline

https://doi.org/10.1017/S0016756821000388 Published online by Cambridge University Press

compositions (e.g. Romano *et al.* 2018; Chen *et al.* 2019). The fertility imparted by this localized metasomatism in the lithosphere may have played a role in permitting a second episode of melting that facilitated this transition. This phenomenon was restricted to the southern limits of the Nain Batholith because it had encountered a comparatively higher volume of slab 'traffic', creating a persistent region of enrichment in the subcontinental lithospheric mantle (e.g. Goodenough *et al.* 2002; Moreno *et al.* 2016). The precise trigger for the second episode of melting is uncertain, but may be attributable to: (1) a final discrete pulse of magmatism, originating in a similar fashion to the Nain Batholith's other constituent plutons, but from a lower initial partial melt fraction; or (2) partial melting of a source in the lower crust, cogenetic with the older Three Bays Pluton, in response to the waning stages of a thermal anomaly that had been responsible for sustaining magmatism to that point, and including a contribution from mantle-fluxed volatiles.

This spatially constrained lithotectonic control does not necessarily function as an explanation for other peralkaline bodies in Labrador, which are distributed along a roughly N–S-oriented lineament. Siegel *et al.* (2017) attribute this to similar pre-enrichment of the lithospheric mantle underlying the Core Zone during the formation of the New Quebec Orogen. This suggests that these complexes were not the products of a unified regional pulse of peralkaline magmatism, and may instead reflect more localized influences. The processes which underlie AMCG complex genesis – requiring an initial, mantle-derived basaltic melt emplaced in an extensional setting – may simply be close enough in principle to those favourable to peralkaline magmatism to have facilitated the transition in Labrador under a generous range of conditions. The polycyclic tectonic history common to many Proterozoic orogens (Watson, 1976; Kröner, 1991), but absent from the Nain Plutonic Suite, may have played a role in obscuring or suppressing this relationship elsewhere. Further work targeting some of the less-studied peralkaline intrusions in Labrador is needed to fully qualify their relationship to regional AMCG-affinity magmatism.

**Acknowledgements.** We thank A Indares, A Borst, K Goodenough, BR Frost and D Lentz for their constructive reviews and many helpful suggestions for improvements to the manuscript. This project was supported by the Grants and Contributions program of the Geological Survey of Canada GEM-2 initiative.

## References

**Anderson IC, Frost CD and Frost BR** (2003) Petrogenesis of the Red Mountain pluton, Laramie anorthosite complex, Wyoming: implications for the origin of A-type granite. *Precambrian Research* **124**(2-4), 243–67.

**Ashwal LD** (1993) *Anorthosites*. Berlin: Springer-Verlag, 422 p.

**Ashwal LD and Bybee GM** (2017) Crustal evolution and the temporality of anorthosites. *Earth Science Reviews* **173**, 307–30.

**Barker F, Wones DR, Sharp WN and Desborough GA** (1975) The Pikes Peak Batholith, Colorado Front Range, and a model for the origin of the gabbro-anorthosite-syenite-potassic granite suite. *Precambrian Research* **2**, 97–160.

**Bartels A, Nielsen TFD, Lee SR and Upton BGJ** (2015) Petrological and geochemical characteristics of Mesoproterozoic dyke swarms in the Gardar Province, South Greenland: evidence for a major sub-continental lithospheric mantle component in the generation of the magmas. *Mineralogical Magazine* **79**, 909–39.

**Bédard JH** (2009) Parental magmas of Grenville Province massif-type anorthosites, and conjectures about why massif anorthosites are restricted to the Proterozoic. *Earth and Environmental Science Transactions of the Royal Society of Edinburgh* **100**(1-2), 77–103.

**Blaxland AB and Parsons I** (1975) Age and origin of the Klokken gabbro-syenite intrusion, South Greenland: Rb-Sr study. *Bulletin of the Geological Society of Denmark* **24**, 27–32.

**Borst AM, Waight TE, Finch AA, Storey M and Le Roux PJ** (2019) Dating agpaitic rocks: A multi-system (U/Pb, Sm/Nd, Rb/Sr and 40Ar/39Ar) isotopic study of layered nepheline syenites from the Ilìmaussaq complex, Greenland. *Lithos* **324–25**, 74–88.

**Bowen NL** (1917) The problem of the anorthosites. *The Journal of Geology* **25**, 209–43.

**Bowen NL** (1945) Phase equilibria bearing on the origin and differentiation of alkaline rocks. *American Journal of Science* **243**, 75–89.

**Bridgwater D** (1967) Feldspathic inclusions in the Gardar igneous rocks of South Greenland and their relevance to the formation of major anorthosites in the Canadian Shield. *Canadian Journal of Earth Sciences* **4**, 995–1014.

**Bybee GM, Ashwal LD, Shirey SB, Horan M, Mock T and Andersen TB** (2014) Pyroxene megacrysts in Proterozoic anorthosites: implications for tectonic setting, magma source and magmatic processes at the Moho. *Earth Planetary Science Letters* **389**, 74–85.

**Cadman AC, Heaman L, Tarney J, Wardle R and Krogh TE** (1993) U–Pb geochronology and geochemical variation within two Proterozoic mafic dyke swarms, Labrador. *Canadian Journal of Earth Sciences* **30**, 1490–504.

**Cadman AC, Tarney J, Baragar WRA and Wardle RJ** (1994) Relationship between Proterozoic dykes and associated volcanic sequences: evidence from the Harp Swarm and Seal Lake Group, Labrador, Canada. *Precambrian Research* **68**, 357–74.

**Charlier B, Duchesne JC, Vander Auwera J, Storme JY, Maquil R and Longhi J** (2010) Polybaric fractional crystallization of high-alumina basalt parental magmas in the Egersund-Ogna massif-type anorthosite (Rogaland, SW Norway) constrained plagioclase and high-alumina orthopyroxene megacrysts. *Journal of Petrology* **51**, 2515–64.

**Chen C, Liu Y, Feng L, Foley SF, Zhou L, Ducea MN and Hu Z** (2018) Calcium isotope evidence for subduction-enriched lithospheric mantle under the northern North China Craton. *Geochimica Cosmochimica Acta* **238**, 55–67.

**Chen J-Y, Yang J-H and Zhang J-H** (2019) Origin of Cretaceous aluminous and peralkaline A-type granitoids in northeastern Fujian, coastal region of southeastern China. *Lithos* **340**, 223–38.

**Collerson KD** (1982) Geochemistry and Rb-Sr geochronology of associated Proterozoic peralkaline and subalkaline anorogenic granites from Labrador. *Contributions to Mineralogy and Petrology* **81**, 126–47.

**Connelly JN and Ryan B** (1996) Late Archean evolution of the Nain Province, Nain, Labrador: imprint of a collision. *Canadian Journal of Earth Science* **33**, 1325–42.

**Corrigan D and Hanmer S** (1997) Anorthosites and related granitoids in the Grenville orogeny: A product of convective removal of the lithosphere? *Geology* **25**, 61–64.

**Corrigan D, Rivers T and Dunning G** (2000) U-Pb constraints for the plutonic and tectonometamorphic evolution of Lake Melville terrane, Labrador and implications for basement reworking in the northeastern Grenville Province. *Precambrian Research* **99**, 65–90.

**Corrigan D and van Breemen O** (1997) U-Pb age constraints for the lithotectonic evolution of the Grenville Province along the Mauricie transect, Quebec. *Canadian Journal of Earth Sciences* **34**, 299–316.

**Creaser RA, Price RC and Wormald RJ** (1991) A-type granites revisited: assessment of a residual-source model. *Geology* **19**, 163–166.

**Dostal J** (2016) Rare metal deposits associated with alkaline/peralkaline igneous rocks. *Reviews in Economic Geology* **18**, 33–54.

**Duchesne JC, Liégois JP, Vander Auwera J and Longhi J** (1999) The crustal tongue melting model and the origin of massive anorthosites. *Terra Nova* **11**, 100–5.

**Duchesne JC, Shumlyanskyy L and Mytrokhyn OV** (2017) The jotunite of the Korosten AMCG complex (Ukrainian shield): crust- or mantle-derived? *Precambrian Research* **299**, 58–74.

**Duchesne JC and Wilmart E** (1997) Igneous charnockites and related rocks from the Bjerkreim–Sokndal layered intrusion (Southwest Norway): a jotunite (hypersthene monzodiorite)-derived A-type granitoid suite. *Journal of Petrology* **38**(3), 337–69.

**Eby GN** (1992) Chemical subdivision of the A-type granitoids: petrogenetic and tectonic implications. *Geology* **20**, 641–44.

https://doi.org/10.1017/S0016756821000388 Published online by Cambridge University Press

**Emslie RF** (1978) Anorthosite massifs, rapakivi granites, and late Proterozoic rifting of North America. *Precambrian Research* **7**(1), 61–98.

**Emslie RF, Hamilton MA and Thériault RJ** (1994) Petrogenesis of a Mid-Proterozoic anorthosite-mangerite-charnockite-granite (AMCG) complex: isotopic and chemical evidence from the Nain Plutonic Suite. *The Journal of Geology* **102**, 539–58.

**Emslie RF and Hegner E** (1993) Reconnaissance isotopic geochemistry of anorthosite mangerite-charnockite-granite (AMCG) complexes, Grenville Province, Canada. *Chemical Geology* **106**(3-4), 279–98.

**Emslie RF and Loveridge WD** (1992) Fluorite-bearing Early and Middle Proterozoic granites, Okak Bay area, Labrador: geochronology, geochemistry and petrogenesis. *Lithos* **28**(2), 87–109.

**Emslie RF and Stirling JA** (1993) Rapakivi and related granitoids of the Nain Plutonic Suite; geochemistry, mineral assemblages and fluid equilibria. *The Canadian Mineralogist* **31**, 821–47.

**Frost BR and Frost CD** (2008a) A geochemical classification for feldspathic igneous rocks. *Journal of Petrology* **49**, 1955–69.

**Frost BR and Frost CD** (2008b) On charnockites. *Gondwana Research* **13**, 30–44.

**Frost CD and Frost BR** (1997) Reduced rapakivi-type granites: the tholeiite connection. *Geology* **25**, 647–50.

**Frost CD and Frost BR** (2011) On ferroan (A-type) granitoids: their compositional variability and modes of origin. *Journal of Petrology* **52**(1), 39–53.

**Frost CD and Frost BR** (2013) Proterozoic ferroan feldspathic magmatism. *Precambrian Research* **228**, 151–63.

**Frost CD, Frost BR, Chamberlain KR and Edwards BR** (1999) Petrogenesis of the 1.43 Ga Sherman batholith, SE Wyoming, USA: a reduced, rapakivi-type anorogenic granite. *Journal of Petrology* **40**(12), 1771–802.

**Frost CD, Frost BR, Lindsley DH, Chamberlain KR, Swapp SM and Scoates JS** (2010) Geochemical and isotopic evolution of the anorthositic plutons of the Laramie anorthosite complex: explanations for variations in silica activity and oxygen fugacity of massif anorthosites. *The Canadian Mineralogist* **48**, 925–46.

**Gandhi SS, Grasty RL and Grieve RAF** (1969) The geology and geochronology of the Makkovik Bay area, Central Mineral Belt, Labrador. *Canadian Journal of Earth Sciences* **6**, 1019–34.

**Gargi SP** (2019) Measuring the decay constant of 87Rb: is the decay in radioisotopes linear? Manifestation and disintegration of the matter in space-time, and age of the Universe. *Solid Earth Sciences* **4**, 12–26.

**Goodenough KM, Upton BGJ and Ellam RM** (2002) Long-term memory of subduction processes in the lithospheric mantle: evidence from the geochemistry of basic dykes in the Gardar Province of south Greenland. *Journal of the Geological Society, London* **159**, 705–14.

**Gower CF, Hall J, Kilfoil GJ, Quinlan GM and Wardle RJ** (1997) Roots of the Labradorian orogen in the Grenville Province in southeast Labrador: evidence from marine, deep-seismic reflection data. *Tectonics* **16**, 795–809.

**Gower CF and Krogh TE** (2002) A U–Pb geochronological review of the Proterozoic history of the eastern Grenville Province. *Canadian Journal of Earth Sciences* **39**, 795–829.

**Hanmer S, Corrigan D, Pehrsson S and Nadeau L** (2000) SW Grenville province, Canada: the case against post-1.4 Ga accretionary tectonics. *Tectonophysics* **319**, 33–51.

**Hill JD** (1982) Geology of the Flowers River-Notakwanon River area, Labrador. St John's: Newfoundland Department of Mines and Energy, Mineral Development Division, Report 81-8.

**Hill JD** (1988) Alkalic to transitional ferrogabbro magma associated with Paleohelikian anorthositic plutons in the Flowers River area, southeastern Nain igneous complex, Labrador. *Contributions to Mineralogy and Petrology* **99**, 113–25.

**Hill JD** (1991) Emplacement and tectonic implications of the Mid-Proterozoic peralkaline Flowers River Igneous Suite, north-central Labrador. *Precambrian Research* **49**, 217–27.

**Hinchey A and Corrigan D** (2019) Geological setting of the Ingrid Group, Labrador. Canada: Newfoundland and Labrador Department of Natural Resources, Current Research, Geological Survey Report 19-1, 147–156.

**Hinze WJ, Allen DJ, Braille LW and Mariano J** (1997) The Midcontinent rift system: a major Proterozoic continental rift. *Geological Society of America Special Papers* **312**, 7–35.

**Hoffman PF** (1989) Speculations on Laurentia's first gigayear (2.0 to 1.0 Ga). *Geology* **17**, 135–38.

**Hynes A and Rivers T** (2010) Protracted continental collision—evidence from the Grenville orogen. *Canadian Journal of Earth Sciences* **47**, 591–620.

**Kerr A** (2011) Rare earth element (REE) mineralization in Labrador: A review of known environments and the geological context of current exploration activity. Canada: Newfoundland and Labrador Department of Natural Resources, Current Research, Geological Survey Report 11-1, 109–43.

**Kerr A** (2014) Sm-Nd isotopic geochemistry of rare-earth-element (REE) mineralization and associated peralkaline granites of the Strange Lake Intrusion, Labrador. Canada: Newfoundland and Labrador Department of Natural Resources, Current Research, Geological Survey Report 15-1, 63–83.

**Kerr A and Smith JL** (2000) Magmatic Ni-Cu sulphide mineralization in the Harp Lake intrusive suite, central Labrador. Canada: Newfoundland and Labrador Department of Natural Resources, Current Research, Geological Survey Report 2000-1, 311–34.

**Kovalenko VI, Naumov VB, Girnis AV, Dorofeeva VA and Yarmolyuk VV** (2006) Peralkaline silicic melts of island arcs, active continental margins, and intraplate continental settings: evidence from the investigation of melt inclusions in minerals and quenched glasses of rocks. *Petrology* **17**, 410–28.

**Kramm U and Kogarko LN** (1994) Nd and Sr isotope signatures of the Khibina and Lovozero agpaitic centres, Kola Alkaline province, Russia. *Lithos* **32**, 225–42.

**Kröner A** (1991) Tectonic evolution in the Archaean and Proterozoic. *Tectonophysics* **187**, 393–410.

**Larsen LM and Sørensen H** (1987) The Ilímaussaq intrusion—progressive crystallization and formation of layering in an agpaitic magma. In *Alkaline Igneous Rocks* (eds JG Fitton and BGJ Upton), pp. 473–88. Geological Society of London, Special Publication no. 30.

**Le Maitre RW, Streckeisen A, Zanettin B, Le Bas MJ, Bonin B and Bateman P** (2005) *Igneous Rocks: A Classification and Glossary of Terms: Recommendations of the International Union of Geological Sciences Subcommission on the Systematics of Igneous Rocks*. Cambridge: Cambridge University Press.

**Lehmann J, Bybee GM, Hayes B, Owen-Smith TM and Belyanin G** (2020) Emplacement of the giant Kunene AMCG complex into a contractional ductile shear zone and implications for the Mesoproterozoic tectonic evolution of SW Angola. *International Journal of Earth Sciences* **109**, 1463–85.

**Longhi J** (2005) A mantle or mafic crustal source for Proterozoic anorthosites? *Lithos* **83**(3-4),183–98.

**Longhi J, Auwera JV, Fram MS and Duchesne JC** (1999) Some phase equilibrium constraints on the origin of Proterozoic (massif) anorthosites and related rocks. *Journal of Petrology* **40**(2), 339–62.

**Ludwig KR** (2003) *ISOPLOT 3.00: A Geochronology Toolkit for Microsoft Excel*. Berkeley: Berkeley Geochronological Centre, Special Publication, 70 p.

**Magaji SS, Martin RF, Ike EC and Ikpokonte AE** (2011) The Geshere syenite-peralkaline granite pluton; a key to understanding the anorogenic Nigerian Younger Granites and analogues elsewhere. *Periodico di Mineralogia* **80**, 199–215.

**Markl G, Marks MA and Frost BR** (2010) On the controls of oxygen fugacity in the generation and crystallization of peralkaline melts. *Journal of Petrology* **51**, 1831–47.

**Marks MA and Markl G** (2017) A global review on agpaitic rocks. *Earth-Science Reviews* **173**, 229–58.

**Martin RF** (2006) A-type granites of crustal origin ultimately result from open-system fenitization-type reactions in an extensional environment. *Lithos* **91**, 125–36.

**Martin RF, Sokolov M and Magaji SS** (2012) Punctuated anorogenic magmatism. *Lithos* **152**, 132–40.

**McCreath JA, Finch AA, Simonsen SL, Donaldson CH and Armour-Brown A** (2012) Independent ages of magmatic and hydrothermal activity in alkaline igneous rocks: The Motzfeldt Centre, Gardar Province, South Greenland. *Contributions to Mineralogy and Petrology* **163**, 967–82.

**McFarlane CRM and Luo Y** (2012) U-Pb geochronology using 193 nm Excimer LA-ICP-MS optimized for in situ accessory mineral dating in thin sections. *Geoscience Canada* **39**, 158–72.

**McLelland JM, Bickford ME, Hill BM, Clechenko CC, Valley JW and Hamilton MA** (2004) Direct dating of Adirondack massif anorthosite by

https://doi.org/10.1017/S0016756821000388 Published online by Cambridge University Press

U-Pb SHRIMP analysis of igneous zircon: Implications for AMCG complexes. *Geological Society of America Bulletin* **116**, 1299–317.

**McLelland JM, Selleck BW, Hamilton MA and Bickford ME** (2010) Late- to post-tectonic setting of some major Proterozoic anorthosite-mangerite-charnockite-granite (AMCG) suites. *The Canadian Mineralogist* **48**, 729–50.

**Middlemost EAK** (1994) Naming materials in the magma/igneous rock system. *Earth Science Reviews* **37**, 215–24.

**Miller RR** (1992) Preliminary report of the stratigraphy and mineralization of the Nuiklavik volcanic rocks of the Flowers River Igneous Suite. Canada: Newfoundland Department of Mines and Energy, Current Research, Geological Survey Report 92-1, 251–58.

**Miller RR** (1993) Rare-metal mineralization in the Nuiklavik volcanic rocks of the Flowers River Igneous Suite. St John's: Newfoundland Department of Mines and Energy, Current Research, Geological Survey Report 93-1, 363-371.

**Miller RR** (1994) Extreme Na-depletion in the peralkaline volcanic rocks of the middle Proterozoic Flowers River cauldron complex, Labrador. Canada: Newfoundland Department of Mines and Energy, Current Research, Geological Survey Report 94, 233–46.

**Miller RR, Heaman LM and Birkett TC** (1997) U-Pb zircon age of the Strange Lake peralkaline complex: implications for Mesoproterozoic peralkaline magmatism in north-central Labrador. *Precambrian Research* **81**, 67–82.

**Miller RR and Kerr A** (2007) Geochemical data from volcanic rocks of the Flowers River Igneous Suite, Labrador: a supplementary release. Canada: Newfoundland Department of Mines and Energy, Current Research, Geological Survey Report no. 18.

**Mitchell JN, Scoates JS, Frost CD and Kolker A** (1996) The geochemical evolution of anorthosite residual magmas in the Laramie anorthosite complex, Wyoming. *Journal of Petrology* **37**, 637–60.

**Moreno JA, Molina JF, Bea F, Abu Anbar M and Montero P** (2016) Th-REE- and Nb-Ta-accessory minerals in post-collisional Ediacaran felsic rocks from the Katerina Ring Complex (S. Sinai, Egypt): an assessment for the fractionation of Y/Nb, Th/Nb, La/Nb and Ce/Pb in highly evolved A-type granites. *Lithos* **258–259**, 173–96.

**Morse SA** (1982) A partisan review of Proterozoic anorthosites. *American Mineralogist* **67**, 1087–100.

**Morse SA** (1991) Basaltic magma from the crust is not a free option. *Transactions of the American Geophysical Union* **72**, 161.

**Myers JS, Voordouw RJ and Tettelaar TA** (2008) Proterozoic anorthosite-granite Nain batholith: structure and intrusion processes in an active lithosphere-scale fault zone, northern Labrador. *Canadian Journal of Earth Sciences* **45**, 909–34.

**Poli S** (2015) Carbon mobilized at shallow depths in subduction zones by carbonatitic liquids. *Nature Geoscience* **8**, 633–36.

**Rivers T and Corrigan D** (2000) Convergent margin on southeastern Laurentia during the Mesoproterozoic: tectonic implications. *Canadian Journal of Earth Sciences* **37**, 359–83.

**Romano P, Andújar J, Scaillet B, Romengo N, di Carlo I and Rotolo SG** (2018) Phase equilibria of pantelleria trachytes (Italy): constraints on pre-eruptive conditions and on the metaluminous to peralkaline transition in silicic magmas. *Journal of Petrology* **59**, 559–88.

**Ryan B** (1991) Makhavinekh Lake pluton, Labrador, Canada: geological setting, subdivisions, mode of emplacement, and a comparison with Finnish rapakivi granites. *Precambrian Research* **51**, 193–225.

**Ryan B** (2000) The Nain-Churchill boundary and the Nain Plutonic Suite: a regional perspective on the geologic setting of the Voisey's Bay Ni-Cu-Co deposit. *Economic Geology* **95**, 703–24.

**Ryan B, Connelly J and James D** (2017) U-Pb geochronology of the western part of the Nain Plutonic Suite, Kingurutik Lake area (NTS 14D/15). Canada: Newfoundland and Labrador Department of Natural Resources, Current Research, Geological Survey Report 17-1, 41–60.

**Salvi S and Williams-Jones AE** (1996) The role of hydrothermal processes in concentrating high-field strength elements in the Strange Lake peralkaline complex, northeastern Canada. *Geochimica et Cosmochimica Acta* **60**(11), 1917–32.

**Sappin AA, Constantin M and Clark T** (2011) Origin of magmatic sulfides in a Proterozoic island arc – an example from the Portneuf-Mauricie Domain, Grenville Province, Canada. *Mineralium Deposita* **46**, 211–37.

**Schärer U, Wilmart E and Duchesne JC** (1996) The short duration and anorogenic character of anorthosite magmatism: U-Pb dating of the Rogaland complex, Norway. *Earth and Planetary Science Letters* **139**, 335–50.

**Scoates JS and Chamberlain KR** (2002) Geochronologic, geochemical and isotopic constraints on the origin of monzonitic and related rocks in the Laramie anorthosite complex, Wyoming, USA. *Precambrian Research* **124**, 269–304.

**Scoates JS, Frost CD, Mitchell JN, Lindsley DH and Frost BR** (1996) Residual-liquid origin for a monzonitic intrusion in a mid-Proterozoic anorthosite complex: the Sybille intrusion, Laramie anorthosite complex, Wyoming. *Geological Society of America Bulletin* **108**, 1357–71.

**Seifert KE, Dymek RF, Whitney PR and Haskin LA** (2010) Geochemistry of massif anorthosite and associated rocks, Adirondack Mountains, New York. *Geosphere* **6**(6), 855–99.

**Shellnutt JG and Zhou M-F** (2007) Permian peralkaline, peraluminous and metaluminous A-type granites in the Panxi district, SW China: their relationship to the Emeishan mantle plume. *Chemical Geology* **243**, 286–316.

**Siegel K, Williams-Jones AE and Stevenson R** (2017) A Nd- and O-isotope study of the REE-rich peralkaline Strange Lake granite: implications for Mesoproterozoic A-type magmatism in the Core Zone (NE-Canada). *Contributions to Mineralogy and Petrology* **172**, 1–23.

**Slagstad T, Roberts NMW, Coint N, Høy I, Sauer S, Kirkland CL, Marker M, Røhr TS, Henderson IHC, Stormoen MA, Skår Ø, Sørenson BE and Bybee G** (2018) Magma-driven, high-grade metamorphism in the Sveconorwegian Province, southwest Norway, during the terminal stages of Fennoscandian Shield evolution. *Geosphere* **14**, 861–82.

**Smith DR, Noblett J, Wobus RA, Unruh D, Douglass J, Beane R, Davis C, Goldman S, Kay G, Gustavson B, Saltoun B and Stewart J** (1999) Petrology and geochemistry of late-stage intrusions of the A-type, mid-Proterozoic Pikes Peak batholith (Central Colorado, USA): implications for petrogenetic models. *Precambrian Research* **98**, 271–305.

**Sørensen H** (1992) Agpaitic nepheline syenites: A potential source of rare elements. *Applied Geochemistry* **7**, 417–27.

**Strong DF and Taylor RP** (1984) Magmatic-subsolidus and oxidation trends in composition of amphiboles from silica-saturated peralkaline igneous rocks. *Tschermaks mineralogische und petrographische Mitteilungen* **32**(4), 211–22.

**Sun SS and McDonough WF** (1989) Chemical and isotopic systematics of oceanic basalts: implications for mantle composition and processes. In *Magmatism in the Ocean Basins* (eds AD Saunders and MJ Norry), pp. 313–45. Geological Society of London, Special Publication no. **42**.

**Upton BGJ** (2013) Tectono-magmatic evolution of the younger Gardar southern rift, South Greenland. *Geological Survey of Denmark and Greenland Bulletin* **29**, 124.

**Upton BGJ, Emeleus CH, Heaman LM, Goodenough KM and Finch AA** (2003) Magmatism of the mid-Proterozoic Gardar Province, South Greenland: chronology, petrogenesis and geological setting. *Lithos* **68**, 43–65.

**van Gool JA, Connelly JN, Marker M and Mengel FC** (2002) The Nagssugtoqidian Orogen of West Greenland: tectonic evolution and regional correlations from a West Greenland perspective. *Canadian Journal of Earth Sciences* **39**, 665–86.

**Vander Auwera J, Bolle O, Bingen B, Liégeois J-P, Bogaerts M, Duchesne JC, De Waele B and Longhi J** (2011) Sveconorwegian massif-type anorthosites and related granitoids result from post-collisional melting of a continental arc root. *Earth-Science Reviews* **107**, 375–97.

**Vander Auwera J, Longhi J and Duchesne JC** (1998) A liquid line of descent of the jotunite (hypersthene monzodiorite) suite. *Journal of Petrology* **39**, 439–68.

**Vasyukova O and Williams-Jones AE** (2014) Fluoride–silicate melt immiscibility and its role in REE ore formation: evidence from the Strange Lake rare metal deposit, Québec-Labrador, Canada. *Geochimica Cosmochimica Acta* **139**, 110–30.

**Vasyukova O and Williams-Jones AE** (2020) Partial melting, fractional crystallization, liquid immiscibility and hydrothermal mobilization – a 'recipe' for the formation of economic A-type granite-hosted HFSE deposits. *Lithos* **356**, 105300.

https://doi.org/10.1017/S0016756821000388 Published online by Cambridge University Press

**Vigneresse JL** (2005) The specific case of the Mid-Proterozoic Rapakivi granites and associated suite within the context of the Columbia supercontinent. *Precambrian Research* **137**, 1–34.

**Vilalva FCJ, Vlach SRF and Simonetti A** (2016) Chemical and O-isotope compositions of amphiboles and clinopyroxenes from A-type granites of the Papanduva Pluton, South Brazil: insights into late- to post-magmatic evolution of peralkaline systems. *Chemical Geology* **420**, 186–99.

**Villa IM, De Bievre P, Holden NE and Renne PR** (2015) IUPAC-IUGS recommendation on the half-life of $^{87}$Rb. *Geochimica Cosmochimica Acta* **164**, 382–85.

**Waight T, Baker J and Willigers B** (2002) Rb isotope dilution analyses by MC-ICPMS using Zr to correct for mass fractionation: towards improved Rb-Sr geochronology? *Chemical Geology* **186**, 99–116.

**Wasteneys HA, Wardle RJ and Krogh TE** (1996) Extrapolation of tectonic boundaries across the Labrador shelf: U–Pb geochronology of well samples. *Canadian Journal of Earth Sciences* **33**, 1308–24.

**Watson JV** (1976) Vertical movements in Proterozoic structural provinces. *Philosophical Transactions of the Royal Society of London, Series A* **280**, 629–40.

**Whalen JB, Currie KL and Chappell BW** (1987) A-type granites: geochemical characteristics, discrimination and petrogenesis. *Contributions to Mineralogy and Petrology* **95**, 407–19.

**Yang WB, Niu HC, Li NB, Hollings P, Zurevinski S and Xing CM** (2020) Enrichment of REE and HFSE during the magmatic-hydrothermal evolution of the Baerzhe alkaline granite, NE China: Implications for rare metal mineralization. *Lithos* **358**, 105411.

https://doi.org/10.1017/S0016756821000388 Published online by Cambridge University Press